ADVANCED INTELLIGENT SYSTEMS
Open Access
www.advintellsyst.com

Advancement of Electroadhesion Technology for Intelligent and Self-Reliant Robotic Applications

Pandey Rajagopalan, Manikandan Muthu, Yulu Liu, Jikui Luo, Xiaozhi Wang,* and Chaoying Wan**

The growing need for automation in industries has foreseen drastic advancements in the development of soft robotics in the areas of navigation systems, textiles, healthcare, and biometric monitoring. Electroadhesion (EA)-based robotic applications benefit from ultralow power consumption, low maintenance, choices in versatile surfaces, sustainable life cycles, applicability in harsh and vacuum environments, and exteroceptive/proprioceptive abilities. It is of scientific and technological importance to comprehend the sequence of developments in working mechanisms, modeling, and materials to explore its full potential for future intelligent robotics systems. This review provides an all-inclusive roadmap of EA technology from its inception to unprecedented developments and complex relationships across multidisciplines, viz., robotics, solid and fluid mechanics, electrostatics, haptics, space technologies, nanotechnology, and IoT.

P. Rajagopalan, Y. Liu, J. Luo, X. Wang
College of Information Science and Electronic Engineering
Zhejiang University
Hangzhou 310027, China
E-mail: prajagopalan@zju.edu.cn; xw224@zju.edu.cn

P. Rajagopalan, Y. Liu, J. Luo, X. Wang
International Joint Innovation Center
Zhejiang University
Haining 314400, China

M. Muthu
Department of Mechanical Engineering
Indian Institute of Technology
Indore 452020, India

M. Muthu
Department of Industrial Engineering
Purdue University
West Lafayette 47907, IN, USA

C. Wan
International Institute for Nanocomposites Manufacturing (IINM)
WMG
University of Warwick
Coventry CV4 7AL, UK
E-mail: chaoying.wan@warwick.ac.uk

The ORCID identification number(s) for the author(s) of this article can be found under https://doi.org/10.1002/aisy.202200064.

DOI: 10.1002/aisy.202200064

1. Introduction to Electroadhesion Technology

1.1. Working Principle

Electroadhesion (EA) effect, also known as the Johnsen–Rahbek effect (JR effect), was first reported by two Danish Engineers, Frederik Alfred Johnsen and Knud Rahbek, in the 1920s.[1,2] They observed when a porous electrolytic material was sandwiched between two metal plates with high potential, experienced an adhesion force to one of the metal plates.

EA effect occurs between the two insulating materials upon applying a high voltage across the back electrodes and the plates adhere to each other due to polarization. Permanent polarization is caused by internal molecular dipoles, whereas induced polarization occurs due to a high electric field.[3] Among the frequency-dependent induced polarization, the interfacial and orientation polarization are responsible for the EA effect.[4,5] When a voltage is applied, the opposite electrode feels the Maxwell tensor force due to the formation of equipotential lines, as shown in **Figure 1**. The equipotential field for the θ-component (E_θ) can be expressed by the Maxwell equation, as shown in Equation (1).

$$E_\theta = -\nabla_\theta\left(U_0 - \frac{2U_0\theta}{\pi}\right) = \frac{2U_0}{\pi r} \tag{1}$$

where r is the radius of concentric equipotential field, θ is the angle of equipotential lines of interest, and U_0 is the equipotential field which is a basic structure of the JR effect between a conductive and insulator substrate.[6]

The working mechanism of EA is illustrated in Figure 1. When a high voltage is applied across the electrodes, charge forms at the electrode–dielectric interface based on the polarities of the potential. This leads to the accumulation of opposite polarities in the respective material based on the conductivity. For conductors, charges are free to move and opposite charges readily reach the electrodes. However, insulators form chains of electric dipoles of positive and negative charged species due to restricted moments. This leads to internal twisting of the molecules which are tightly aligned to another molecule (in solids). The resultant force of all internal forces and twisting results in the adhesion of the material. This makes it a universal phenomenon irrespective of the surface nature and can be used for conductors, semiconductors, and insulators. When the resistivity of dielectric films is

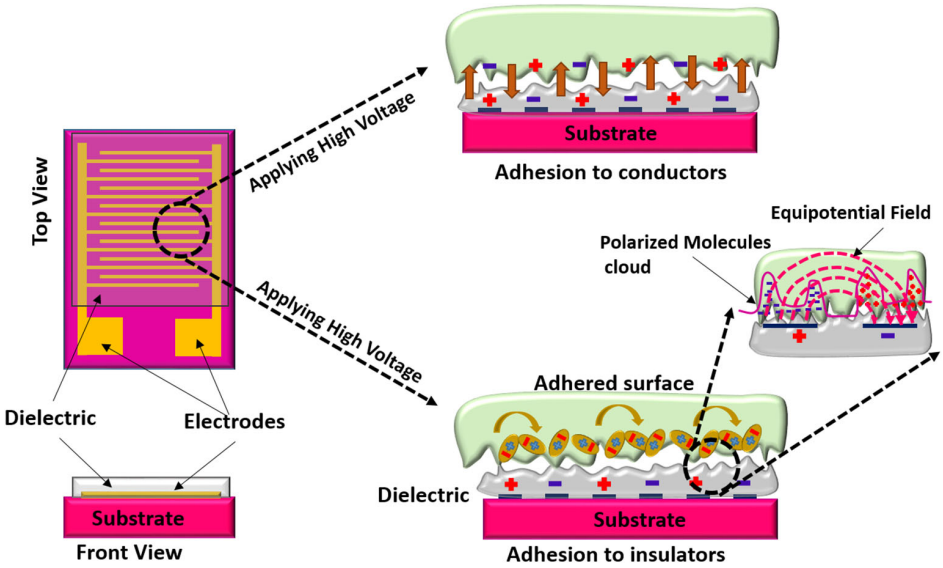

Figure 1. Structure and mechanism of EA: (left) the top view (TV) and front view (FV) of EA device showing the substrate, interdigitated electrode patterns, and the dielectric coating; (right) the principle of adhesion in conducting and insulating solid. When a high voltage is applied to the electrodes, charge formation occurs at the electrode–dielectric interface based on the polarities of the potential. For conductors, charges are free to move and opposite charges readily reach the electrodes. In insulator, materials form a chain of electric dipoles of positive and negative charged species due to restricted motion.

high (insulating characteristics), the clamping force is called the Coulomb force, whereas, in low resistivity (semiconductor or metallic characteristics), it is known as the Johnsen–Rahbek force (JR force).[7] The typical voltage values range from 3 to 5 10 kV for the lifting operation due to which many safety peripheral electronics are added to the gripper. Initially, it was thought to be influenced by a few obvious parameters such as dielectric permittivity, voltage, distance, and roughness. However, with the recent advancements, it was revealed that there are as many as 33 variables to influence the adhesion[8] that are not easy to control and often end up in trading the properties as per the requirements. In a nutshell, the electrodes with opposite polarity attract each other and if any materials come in contact (close enough) with the dielectric-covered electrodes it clings to the surfaces. EA technology requires a substrate (rigid or flexible), pair of electrodes, a dielectric film, and a high voltage supply for prehension.

Table 1 compares the existing technologies of griping with their pros and cons.[9] It is evident that EA has many advantages over conventional gold standard industrial gripper technologies, for example, applicable to almost any surface, tolerant to harsh environments, system simplicity, and very low power requirements. In the coming decade, EA has the great potential to dramatically transform the gripper industries.

In this review, we comprehensively discussed the EA technology development from the historical landmarks fundamental theories to device design and applications. Section 2 provides an overview of the potential contending theories and their background with the modern development of the haptic models. Section 3 discusses the technology advancements in materials, and manufacturing of dielectric and electrodes with the latest trends in modern fabrication methods. Section 4 comments on the prospective applications and the impact of EA on the modern griping industry. Furthermore, the smart EA devices that are responsive and sensitive to external stimuli are discussed in Section 5. Section 6 emphasizes the hybridization of the EA effect with other technologies such as gecko-inspired adhesion, electroactuators, electrowetting, or dielectrophoresis that are promising due to synergistic engagements. Finally, the perspectives and remarks of EA are discussed, with special emphasis on the recent spin-out startups like Grabit Inc. We highlighted the important parameters on the materials and the commercial points and concluded with the future directions of EA technology.

1.2. Historical Roadmap of EA Technology

The major roadmap development of EA technology in the last 100 years is provided in **Figure 2**. During the initial 30 years of invention, the EA technology was energy-intensive and way ahead of its time in a commercial sense. Although a similar technology based on electrostatics was implemented in commercial use in printing, spraying, precipitation, and filtering, there was no significant commercial viability observed for EA technology until the 1950s. In 1953, the first plotter was invented by Remington Rand for overcoming the issue of mechanically holding the paper properly while printing; hence, the EA technology was found to be commercially useful in handling large sheets of paper static in the early plotter applications.[10] The early 9125A Flatbed Plotter design is shown in Figure 2. During the late 1950s, C.J. Fitch designed an electrostatic clutch based on the JR effect with a contrasting similarity as Johnsen and Rahbek design, but with an improved response time (3 ms to stop a shaft rotating at 1600 rpm).[11] Figure 2 shows an improved

Table 1. A comparison of the various technologies for gripping and adhesion.

Technology	Advantages	Disadvantages
Conventional mechanical jaw grippers 	Easy to design Can be easily scaled Robust Easy to carry any shape	Difficult for smaller parts Difficult to control the force Not suitable for delicate parts
Magnetic 	For ferromagnetic material High shape selectivity Porous and rough surfaces	Suitable only for magnetic materials Leads to the magnetization of parts Not suitable for very small parts Difficult to position
van der Walls 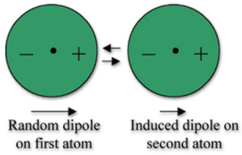	Reliable Can stick most materials Suitable for very flat surfaces	Difficult to control the forces Release is difficult Costly and prone to wear and tear Rough surfaces are difficult to grip
Vacuum 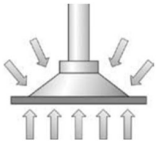	Well established in the industry Suitable for small to very large structures Low maintenance	Not suitable for very complex shapes Not suitable for porous or very rough structures Not suitable for vacuum or space applications
Soft hydraulic/pneumatic 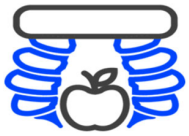	High shape selectivity Can be used for delicate parts Suitable for IoT-based applications Cost-effective	Low force generation Prone to wear and tear
Shape memory alloys/polymers 	Among the most recent developed technology Usually robust	Expansive Slow Lower degree of actuation
Electroadhesion (Reproduced with permission.[59] Copyright 2015, Wiley) 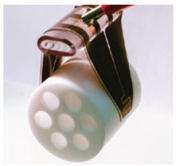	Suitable for all materials Suitable for delicate parts Low energy requirements Suitable for harsh and vacuum environments Exteroceptive/proprioceptive	Low force Coupling/decoupling takes time Humidity affects the coupling

electrostatic clutch design for faster printing technology patented by Landon et al.[12].

In the early 1950s, Edward Mallinckrodt designed the haptic-based devices where an alternating current in dielectric covered electrodes gives the periodic adhesion and repulsion that become the benchmark for modern-day responsive tactile screens and touch pads. In the early 1960s, NASA launched the Gemini space flight missions which constitute a sum of 19 launches, including 10 crewed missions.[13] During these early missions, the research emphasis was focused on the positioning and stability of astronauts in low or zero-gravity conditions in and out of spacecraft and stations. These visits were mainly for either repair work or to undertake some experiments in outer space. As these spacecrafts were made of nonferrous materials like titanium, carbon composites, or aluminum, there was a pressing requirement for nonmagnetic adhesion technology like EA technology. Due to external vacuum in space and nonferrous requirements, both magnetic and vacuum technologies were redundant; the EA research has become the basis of handling complex and nonmagnetic airplane parts in the aerospace industry.[14] Figure 2 shows the various EA-based devices developed at the Chrysler space division for space explorations.

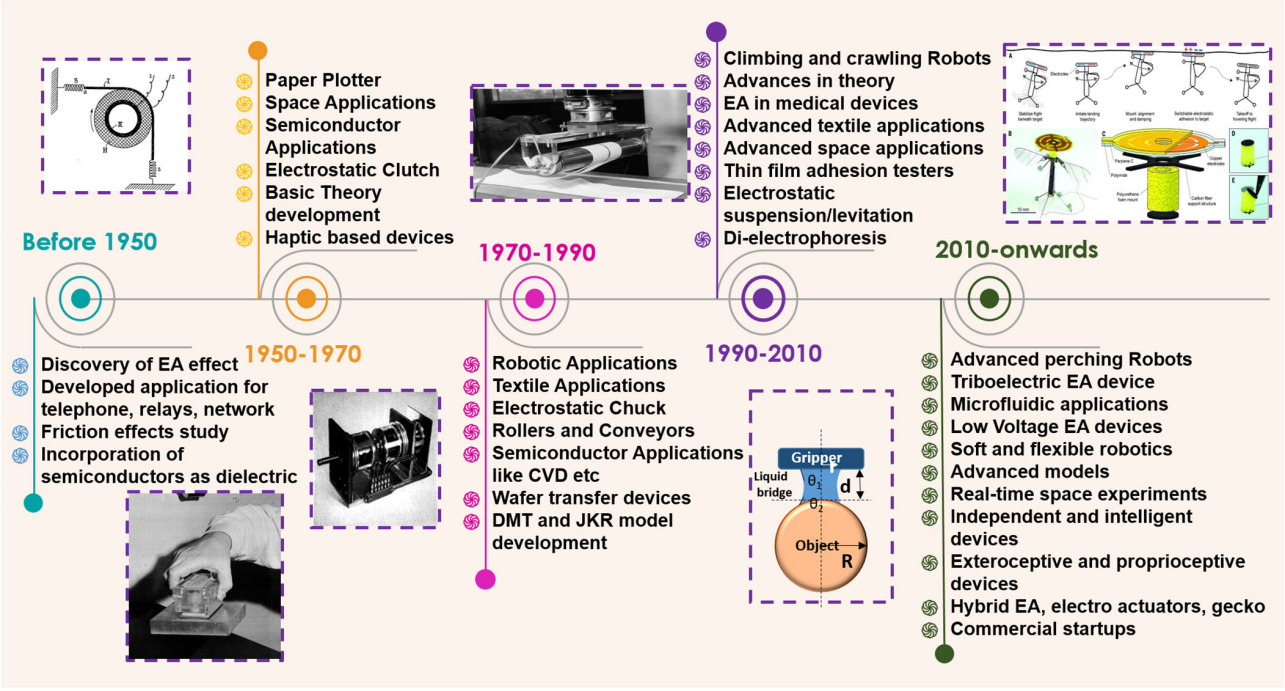

Figure 2. Chronology of milestones achieved in the EA research in the last 100 years. Reproduced with permission.[117] Copyright 2017, AAAS.

Semiconductor industries were in the early days of their inception in the early 1970s and progress was made in silicon-based electronic devices for computer chip applications.[15] Automatic handling of silicon wafers was proving to be a challenge for the industry; hence, the EA technology was extended to the semiconductors as electrostatic chucks.[16] Moreover, the vacuum chuck which is an alternative technology has limitations in a variety of semiconductor processing, while the wafer transfer technique based in EA was incorporated into chemical vapour deposition (CVD) processes to electrostatically move and precisely place the wafers without the need for bulky holders.[17,18] Within a decade or so, EA was introduced to a variety of robotic applications like textile fibers handling and the layup process of composite fibers.[19,20] This led to the development of EA conveyor platforms in the 1990s and was useful for the textile industry. In the 21st century, EA technology rapidly gained more attention in hybridization with other technologies such as gecko adhesion, electroactuators, wall climber robots, or perching robots.[8] It has not only been implemented in solid object manipulation but also in liquid manipulation, which will be subsequently discussed in the later sections. The advances in analytical models and theory are witnessed in the last two decades and will be discussed in detail. Innovations in EA continued to date and have found exciting applications in the food and agriculture industries, optoelectronics, microfluidic devices, and soft robotics. Modern EA devices are self-reliant as well as smart and multifunctional and will be discussed in subsequent sections. The research of EA technology has consistently increased in the last 60 years, with ≈10% growth of annual publications as shown in **Figure 3**. The theoretical development of EA effects and its modern perspectives are discussed as follows.

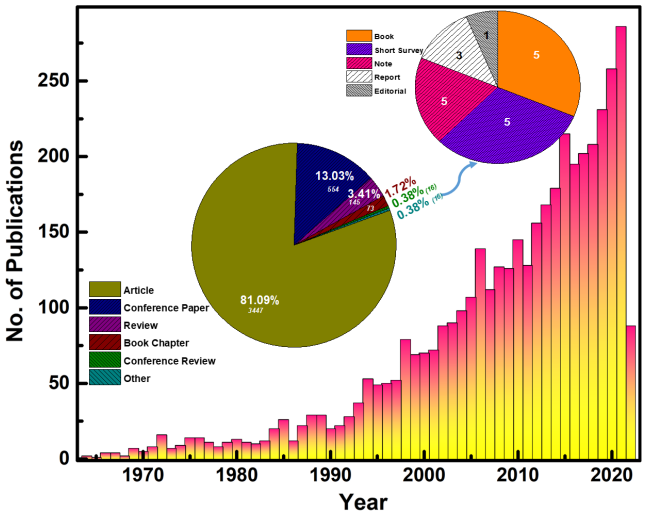

Figure 3. Progress in the field of EA devices over the years. Data provided by Scopus with keywords (electroadhesion) or (electroadhesive) or (electrostatic and adhesion). Inset shows the pie chart for types of publications over the years.

2. Fundamental Theory and Modeling

2.1. Advances in the EA Modeling

Most of the researchers qualitatively anticipated the presence of electrostatic force at the interface; however, the accurate quantitative behavior is difficult to predict due to the complex nature of the electrical, chemical, and mechanical forces present at the

interface. Johnsen and Rahbek observed that the adhesion was roughly following the electrostatic law[2] (with a slight deviation) and is given by Equation (2).

$$\frac{F}{A} = \frac{V_i^2}{8\pi d^2} = \frac{E^2}{8\pi} \tag{2}$$

where F is the force of adhesion, A is the area, V_i is the intersurface potential drop, d is the distance between the surface, and E is the electric field strength. Without going much into the details of deviation, the reason was speculated to be the ambient humidity that alters the resistance of the dielectric. This model based on a parallel plate capacitor is often quoted as the JR model in the literature.[21] Balakrishnan proved that the effect followed the electrostatic law and the humidity has little or no effect on the EA process when examined carefully by using discs of magnesium orthotitanate. Moreover, he suggested that the distance changes with applied voltage which also results in the altered results which were later proved by Fitch as well.[11] Stuckes suggested the presence of field emission effect at the interface. Once the voltage reaches a certain threshold value it results in the nonuniform relation between the force and voltage.[22] It was observed that as the voltage increases, the area of field emission also increases, thus limiting the field strength of the circuit. Hence, the square law is applicable only for a small range and does not increase swiftly after the threshold value is reached. Later, Atkinson improvised the Stuckes model by suggesting that interfacial voltage (V_i) is not a constant function of applied voltage but also depends on the constant internal resistance (R_{int}) and the extent of field emission.[23] This is given by Equation (3)

$$V_i = V - i.R_{int} \tag{3}$$

Hence, after fitting the experimental model he suggested an altered equation as given in Equation (4)

$$\frac{F}{A} = \frac{V_i^2}{88.8 \times 10^{11}.d_{max}^2}\left(1 + 2\ln\frac{V_{max}}{V_i}\right) \tag{4}$$

Livermore suggested that apart from the above parameters, some other parameters such as the surface deformation, temperature of contacting objects, surface ionization, an so on also influence the force voltage relationship.[24] The deformation varies based on the modulus of materials and can be either Hertzian deformation or plastic deformation which was studied using a Fizeau interferometer device between transparent conducting oxide glass and a variety of opaque materials. Surface roughness is another parameter that was investigated and revealed that adhesion decreases significantly with the increase in surface roughness. Along with surface roughness, the curvature of a surface (r) plays a crucial role in the strength of adhesion and is related by Equation (5)

$$E_0 \propto e^{\frac{-CFA}{r}} \tag{5}$$

where CFA is the closed line average (average roughness by stylus profilometer) and r is the radius of curvature. Levermore concluded that the work function of the electrode does not show much significance upon adhesion and the effect of polarity change was observed in faster coupling and decoupling. It is observed that lubricated surface electrodes (surface contamination) increased the current either due to dielectric breakdown or due to changed electrical conductivity. Low pressure changed the ionization potential which affects the adhesion. However, the etching does not play a significant role until the conditions fulfill Paschen's law of breakdown.

The temperature was supposed to decrease the adhesion and was proved by a variety of tests. Temperature change results in the change in resistivity and adsorption (for instance, in carbon, this energy can be as low as 70 °C which is equivalent to 0.5 eV activation energy needed). Chrysler Space Corporation in their detailed study on basic parameters and Levermore's results are aligned with these results. The study at Chrysler demonstrated a prototype for both rigid and flexible EA which is shown in Figure 2. The thickness of the dielectric coating is one of the key parameters in generating appropriate EA properties. It was concluded that thickness is related to resistivity and the chemical constituent of the device material. However, it was observed that thickness-based experimental results were not equated with the theoretical results. In the short-range, the increase in the voltage increases adhesion; however, beyond a certain value, increases the current consumption. It was also said that temperature change (increase/decrease) decreases the adhesion in the Buna-N rubber, which was suggested to be related to the material properties and may not be an actual EA-related property. The coupling/decoupling time is related to the material properties (physical/ chemical) and the chemical identity is the key constituent that results in the appropriate adhesion forces.

However, most of the work was based on simple parallel plate capacitor modeling and was often used for simplistic modeling.[21,25,26] Toshiya et al. worked out on the detailed JR model and found that it worked well for highly resistive samples (insulators) initially, but deviated with the applied time.[27,28] The force increased with the time of applied voltage due to the larger accumulation of the charges (charge density, σ) in the dielectric layer. Moreover, σ varied from place to place; hence, the concentration factor (α) was introduced. The individual resistance of the respective layer and air gap must be added to the model. **Figure 4**a shows the equivalent circuit for the JR model, according to Equation (6)

$$F = \alpha\frac{\sigma^2}{2\varepsilon_0} \tag{6}$$

By analyzing the equivalent circuit, the accumulated charges can be written in terms of conductance as (detailed derivation can be traced here[27]) Equation (7)

$$\sigma = \frac{(G_aC_d - G_dC_a)V}{(G_a + G_d)A}\left\{1 - e^{-\left[\left(\frac{G_a+G_d}{C_a+C_d}\right)t\right]}\right\} \tag{7}$$

where G_a and G_d are the conductance of air gap and dielectric layer, respectively. Note subscript "a" and "d" denotes the respective value of air gap and dielectric, respectively. Now as $F(t)$ is the function of time, hence it can be written as Equation (8)

$$F(t) = F_0T(t) \tag{8}$$

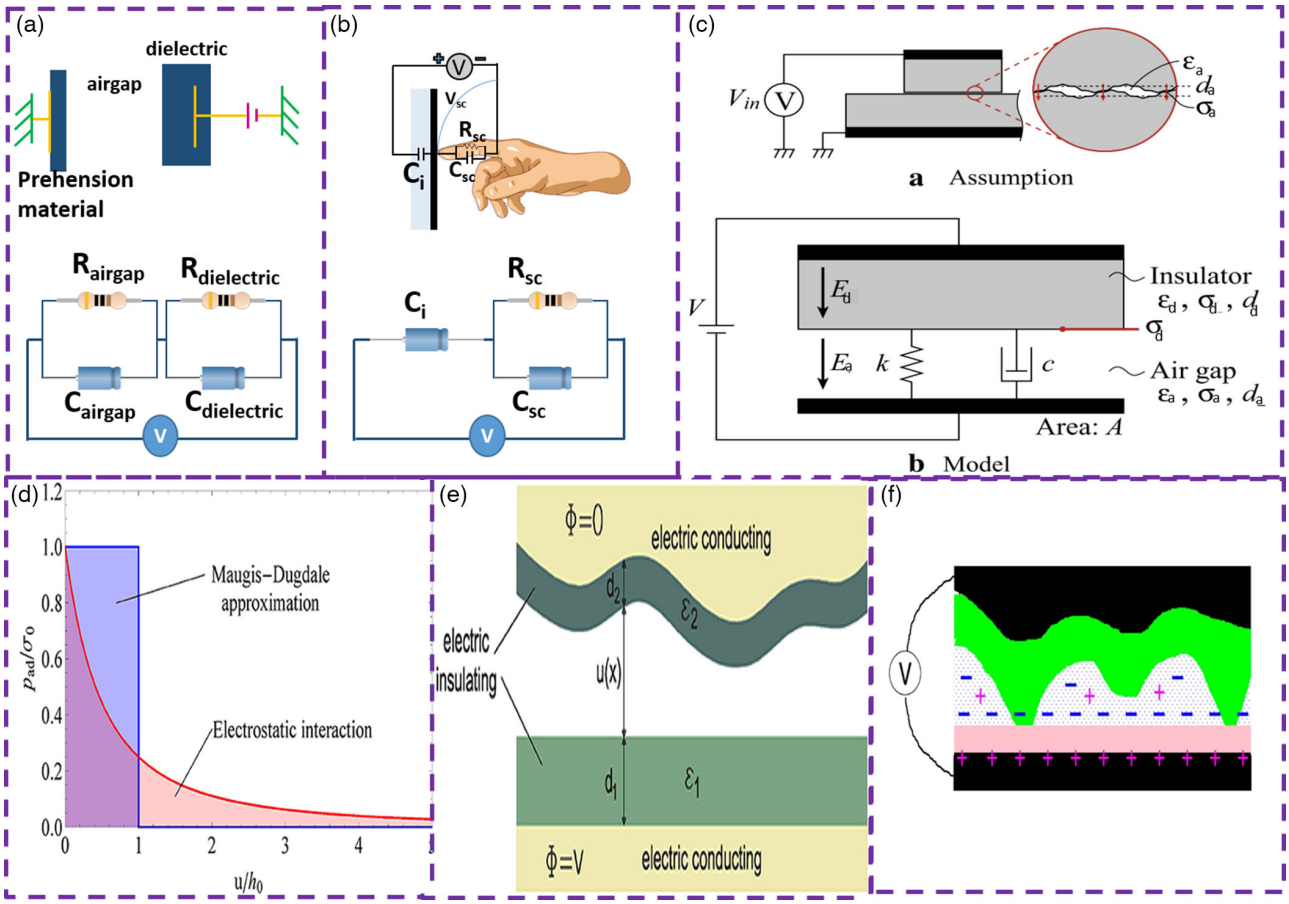

Figure 4. a) Theoretical investigations in EA models: (top) physical interpretation and (bottom) the Johnsen–Rahbek model equivalent circuit diagram.[21] b) (top) The electrical equivalent of the stratum corneum and[30] (bottom) equivalent circuit diagram of the leakage model.[21] (c) Nakamura et al. proposed model with mechanical effects such as spring constant (k) and damping coefficient. Reproduced under the terms and conditions of the CC BY license.[21] Copyright 2017, The Authors. Published by Springer Nature; d) a typical electrostatic attraction force law replaced by a Maugis step function law. Reproduced under the terms and conditions of the CC BY license.[41] Copyright 2020, The Authors. Published by Frontiers Media; e) Ciavarella et al. bearing area model geometry for the rough interfacial surface; here a rough elastic solid is squeezed against a flat rigid solid with the back electrode; f) fluid with ions between a finger (rough) and a touch screen (flat) when the DC field is applied charges moved through the stratum corneum and are screened by ions fluid and the potential drops on the touch screen. Reproduced under the terms and conditions of the CC BY license.[35] Copyright 2021, The Authors. Published by IOP Publishing.

where F_0 is the saturated force after a long time and $T(t)$ is the force function of time; hence, from Equation (6)–(8), we have

$$F(t) = \alpha \frac{V^2}{2\varepsilon_0 A^2} \left(\frac{G_a C_d - G_d C_a}{G_a + G_d} \right)^2 \times \left\{ 1 - e^{-\left[\left(\frac{G_a + G_d}{C_a + C_d} \right) t \right]} \right\}^2 \quad (9)$$

Hence, the residual electrostatic force ($F'(t)$) which remains in the electrode (after the voltage source is removed) can be written as Equation (10)

$$F'(t) = \alpha \frac{V^2}{2\varepsilon_0 A^2} \left(\frac{G_a C_d - G_d C_a}{G_a + G_d} \right)^2 \times \left(e^{-\left[\left(\frac{G_a + G_d}{C_a + C_d} \right) t \right]} \right)^2 \quad (10)$$

Apart from the JR model, the other model that has been intensively considered is the leakage model and is often used in haptic-based modeling to explain the decrease in the force.[29,30] In this model, each electrode has a separate dielectric layer with a single leak resistance which decreases the force. However even after the reproducible result, Akio et al. suggested that the leakage model remains unclear on many grounds and the mechanical behavior needs to be taken into the account along with electrical behavior.[21] Figure 4b shows the equivalent circuit diagram of the leakage model and will be discussed in the next section.

2.2. Recent Advances in Theory to Compensate Mechanical Effects and Generalized Electromechanical Models

The real force calculation is the function of mechanical and electrical responses occurring at the interface which can change the response dynamically. Hence, the model has to be more dynamic to counter the effects of surface roughness, microscopic deformations, humidity, and heat in the device and will be discussed in this section. Nakamura et al. and Chen et al. brought new insights into these advanced models that led to some generalized

models for EA and haptic-based devices.[21,31] It is observed that in the JR effect the adhesion force increases with the DC voltage whereas in the haptics the adhesion decreases with time. Nakamura et al. proposed an electromechanical model with mechanical effects such as spring constant (k) and damping coefficient (c) as shown in Figure 4c to solve the discrepancy. From the Maxwell stress tensor, the EA force can be calculated as Equation (11)

$$F = \frac{1}{2}\varepsilon_a A E_a(t)^2 \tag{11}$$

From the charge conservation equation at the interface, we have Equation (12)

$$J_d - J_a = -\frac{\partial}{\partial t}(\varepsilon_d E_d - \varepsilon_a E_a) \tag{12}$$

where J is the current density in each dielectric. Assuming the Ohm's law holds for the Equation (12) ($J = \sigma E$), we have

$$\sigma_d E_d - \sigma_a E_a = -\frac{d}{dt}(\varepsilon_d E_d - \varepsilon_a E_a) \tag{13}$$

Applying the boundary conditions, $V = E_a d_a + E_d d_d$ to Equation (13), we have

$$(\varepsilon_a d_d + \varepsilon_d d_a)\frac{dE_a}{dx} + (\sigma_a d_d + \sigma_d d_a)E_a = \sigma_d V + \varepsilon_d \frac{dV}{dt} \tag{14}$$

Equation (14) can be modified for both AC and DC cases.
For DC case: for $V = V_0$

$$E_a(t) = \frac{\sigma_d}{\sigma_d d_a + \sigma_a d_d} V_0\left(1 - e^{-\frac{1}{\tau}}\right) + \frac{\varepsilon_d}{\varepsilon_d d_a + \varepsilon_a d_d} V_0 e^{-\frac{1}{\tau}} \tag{15}$$

where τ is the time constant and is given by

$$\tau = \frac{\varepsilon_d d_a + \varepsilon_a d_d}{\sigma_d d_a + \sigma_a d_d} \tag{16}$$

If we take a look at Equation (15), we find that the first term is related to the conductivity (incremental) and the second term is related to the permittivity (detrimental). Hence, if the first term is dominant, it is a case of the JR effect whereas when the latter term is dominant, it results in the hepatic sensor cases. For the dominant term, we need to calculate the interfacial charges ($\sigma_f(t)$) which is given by Equation (17)

$$\sigma_f(t) = -\varepsilon_d E_d + \varepsilon_a E_a(t) = \frac{\sigma_d \varepsilon_a - \sigma_a \varepsilon_d}{\sigma_d \varepsilon_a + \sigma_a \varepsilon_d} V_0\left(1 - e^{-\frac{1}{\tau}}\right) \tag{17}$$

If the initial charge is $\sigma_f(t) \neq 0$, then at $t = 0$, the time-dependent electric field can be written as Equation (18)

$$E_a(t) = \frac{\sigma_d}{\sigma_d d_a + \sigma_a d_d} V_0\left(1 - e^{-\frac{1}{\tau}}\right) + \frac{\varepsilon_d V_0 + \sigma_f(0) d_d}{\varepsilon_d d_a + \varepsilon_a d_d} e^{-\frac{1}{\tau}} \tag{18}$$

It also shows that the EA force depends on the initial accumulated charges (second term of Equation (18)). Hence, when the voltage is turned off, the equation does not end up as a zero-field equation like the earlier cases.

For AC case: for $V = V_0 \sin\omega t$, the electric field can be written as

$$E_a(t) \approx \frac{\varepsilon_d}{\varepsilon_d d_a + \varepsilon_a d_d} V_0 \sin\omega t \tag{19}$$

And the adhesion force can be written as

$$F = \frac{1}{2}\varepsilon_a A E_a(t)^2 = \frac{A}{2\varepsilon_a\left(\frac{d_d}{\varepsilon_d} + \frac{d_a}{\varepsilon_a}\right)^2} V^2 \tag{20}$$

Apart from the analytical model, Donald and Guo et al. have performed the simulation through finite elemental analysis which helps to visualize 2D/3D representation of electric field and forces acting on the substrate.[32,33] Moreover, with the simulation studies, a variety of electrode patterns can be tested before the actual experiment, thus saving resources and improving efficiency. However, many of these studies still could not validate the experimental parameters perfectly due to the mechanical and thermal changes occurring at the interface. Moreover, these models are still at their initial stages of development and require consistent improvisation.

2.3. Developments in Contact Mechanics Models for Haptics and EA

In 1950, Mallinckrodt observed a strange periodic adhesion and repulsion to his finger upon touching the brass electric when the electricity was flowing[34] which became the foundation of haptic devices such as tactile sensors and touchscreens.[35] In a simple touchscreen-based device, the screen contains lines of transparent conducting oxide covered with a thin layer of silicon dioxide. When one touches the screen, some charges may transfer from the finger to the screen and eventually decreases the current locally which can be detected by the sensors located in the periphery of the screen. In haptic devices, an alternating voltage is applied to the capacitive screen which gives the sensory touch to the user, thus making a simple screen into a responsive and active device due to the generated EA forces. The simple response of adhesion can be turned into a rich variety of signatures by altering the amplitude, frequency, gap, electrode pattern, and waveform of the signal and can be a useful tool for visually impaired people. Grimnes investigated the effects on the skin and coined this phenomenon as electrovibration.[36] Researchers investigated and optimized the procedure for psychophysiological evaluations by altering the amplitude, gap, electrode pattern, and so on to gain the desired response from the device.[37]

The surfaces in contact undergo deformation for both EA and haptics, due to normal and frictional stress that acts perpendicular and tangentially to the surface respectively. However, even after intense developments in the theory and experimentation of contact mechanics, the area remains largely debated due to many theories leading to fairly analogous inferences. The interesting and foundation work in this direction comes from an eminent physicist Heinrich Hertz who observed the contact deformation of spherical objects using light.[38] However, a century later Johnson and co-workers found a similar solution for the adhesion elastic contact-based problem as Hertz, and their

model is known as the JKR model (an acronym for Johnson, Kendall, and Roberts, the inventors of this model).[39] However, the proposed theory by Derjaguin and co-workers also known as the DMT model (an acronym for Derjaguin–Muller–Toporov, the inventors of this model) was proposed rejecting the previous JKR model.[40] These two models are often discussed and debated in the contact mechanics as well as the haptic devices for theoretical investigations.[41,42]

In recent years, many researchers worked out the DMT model and used it for the EA technology. Persson et al. proposed the mean-field theory (MFT), based on the DMT assumption accounting for the EA model involving contact mechanics.[40,41,43] The MFT evolved from the van der Walls adhesion and works on two constraints: 1) two electrically conducting films insulated by two separate layers; 2) voltage drops at electrically conducting solids due to contact resistance.[41,43,44] In this model, one surface is kept rigid and smooth (representing touch screen) and the other is rough and soft (representing finger). The pressure/loading *(p)* is the sum of EA stress (averaged in the *z*-direction, p_f) and the external pressure (p_0), $p = p_f + p_0$.

If $P(p,u)$ denotes the probability distribution of the interfacial separation,[45] then

$p = p_0 + V_0^2 \int_0^\infty du P(p,u) G(p,u)$, where $G(p,u) = \sigma_{zz}/V_0^2$ and σ_{zz} is the EA stress from the *zz*-component of the electrostatic Maxwell stress tensor. Alternatively, this equation can be written as $V_0^2 = \frac{p-p_0}{\int_0^\infty du P(p,u) G(p,u)}$, where V_0 is a function of nominal contact pressure p.[35,43] It is interesting to note that in the absence of applied voltage the $p = p_0$ (external applied pressure). Thin screen surface, such as mobile phones, has low leakage current, while for thicker surfaces, the model needs to consider the effects of leakage current. The theory was successfully implemented to model the real contact area of the skin on different surfaces induced by capillary forces and EA independently.[46,47] It also gives directions about the effects of sweaty fingers on the inhibition/screening of the charges. The detailed investigation of sweaty fingers was carried out recently by Shultz et al. and will be discussed subsequently.[48] Michele et al. proposed that MFT was too general involving complex cases, hence was difficult to implement and interpret. They suggested a simpler model based on MFT and DMT approximations known as the bearing area model (BAM) which was completely expressible in simple equations by estimating the geometry of contacts. The general electrostatic potential used in the MFT was replaced by the Maugis–Dugdale equivalent which is defined as a function of the gap *u*, as shown in Figure 4d,e.[49]

$$p_{ad}(u) = \begin{cases} \sigma_0, u \le h_0 \\ 0, u > h_0 \end{cases} \tag{21}$$

Integrating for the nominally flat surface, the work of the adhesion is given by

$$\Delta\gamma = \frac{\varepsilon_0}{2} V^2 \int_0^\infty \left(\frac{1}{u(x)+h_0}\right)^2 du = \frac{\varepsilon_0}{2h_0} V^2 \tag{22}$$

here $h_0 = \frac{d_1}{\varepsilon_1} + \frac{d_2}{\varepsilon_2}$; and for work of the adhesion to be equal to the Maugis–Dugdale approximation, we have $\Delta\gamma = \sigma_0 h_0$, so Equation (22) can be written as[50]

$$\sigma_0 = \frac{\varepsilon_0}{2h_0^2} V^2 \tag{23}$$

For the nominally flat surface with surface roughness (h_{rms}), the key idea is to estimate the correct area which works well for the spherical systems (DMT/JKR).

$$\frac{A_{ad}}{A_0} = \frac{1}{2}\left[erfc\left(\frac{\overline{u}-h_0}{\sqrt{2}h_{rms}}\right) - erfc\left(\frac{\overline{u}}{\sqrt{2}h_{rms}}\right)\right] \tag{24}$$

where $\overline{u}$ is the mean separation of the surfaces, h_{rms} is the root mean square of roughness, and *erfc* is the error complementary function.[50] Later, the model was extended to insulating and conducting solids; the respective detailed calculations can be looked into the publications.[41,49,50] Some other influential and interesting works based on the JKR model, the detailed adhesion mechanics,[51–54] and some new insights on the extent of angstrom level surface roughness, chemical homogeneity, or capillary formation are also reported.[47,54,55]

As mentioned earlier in this section, sweat/oil on the human skin interferes with the EA and electrovibration phenomenon of the device which results in the discrepancy, and thus largely the theoretical model fails to accurately predict the EA/electrovibration in the haptic devices as shown in Figure 4f. Hendriks et al. investigated the effects of environmental factors on the frictional property of skin and calculated the coefficient of friction under various conditions.[56,57] In the secretion and condensation of sweat and other biological fluids, it forms the capillary bridges in the vicinity of the screen which are difficult to predict. In addition, the ambient temperature and relative humidity also influence the output.[46,47,52,55,58]

2.4. Modeling of Electrodes

The discussion above mainly considered the effects of the electric field, dielectric properties, roughness, and surface area on EA. However, if the area is an important factor in the force calculations, then the question arises that why the interdigitated electrodes produce more force compared to single body electrodes[59]? The electric field is a function of both area and geometry which eventually influences the EA forces. Besides, as shown in Figure 1, the equipotential field generated at the interface between the pair of electrodes is hemispherical. This results in the geometrical effects on the output.[60] The gap of electrodes is usually kept as low as possible to enhance the force of adhesion as discussed earlier which is usually limited by the dielectric breakdown. However, design can influence leakage values and electric field distribution which, in turn, influence the adhesion force by as large as 1500%.[61] Although earlier studies were mostly based on experiments, the modern theoretical analysis and FEM software-based numerical simulation would guide the design and fabrication of electrodes.[62]

The electrode geometry and configuration can be optimized to maximize the electric field by using the FEM methods along with analytical software. The first parameter to work upon is the width (due to manufacturing limitations, the authors set it to 0.6 μm).[61] The other dimensions of electrodes are simultaneously varied by MATLAB and systematically studied with the FEM package (COMSOL). Different electrode patterns like IDT, concentric, Hilbert, and spiral were studied, as shown in

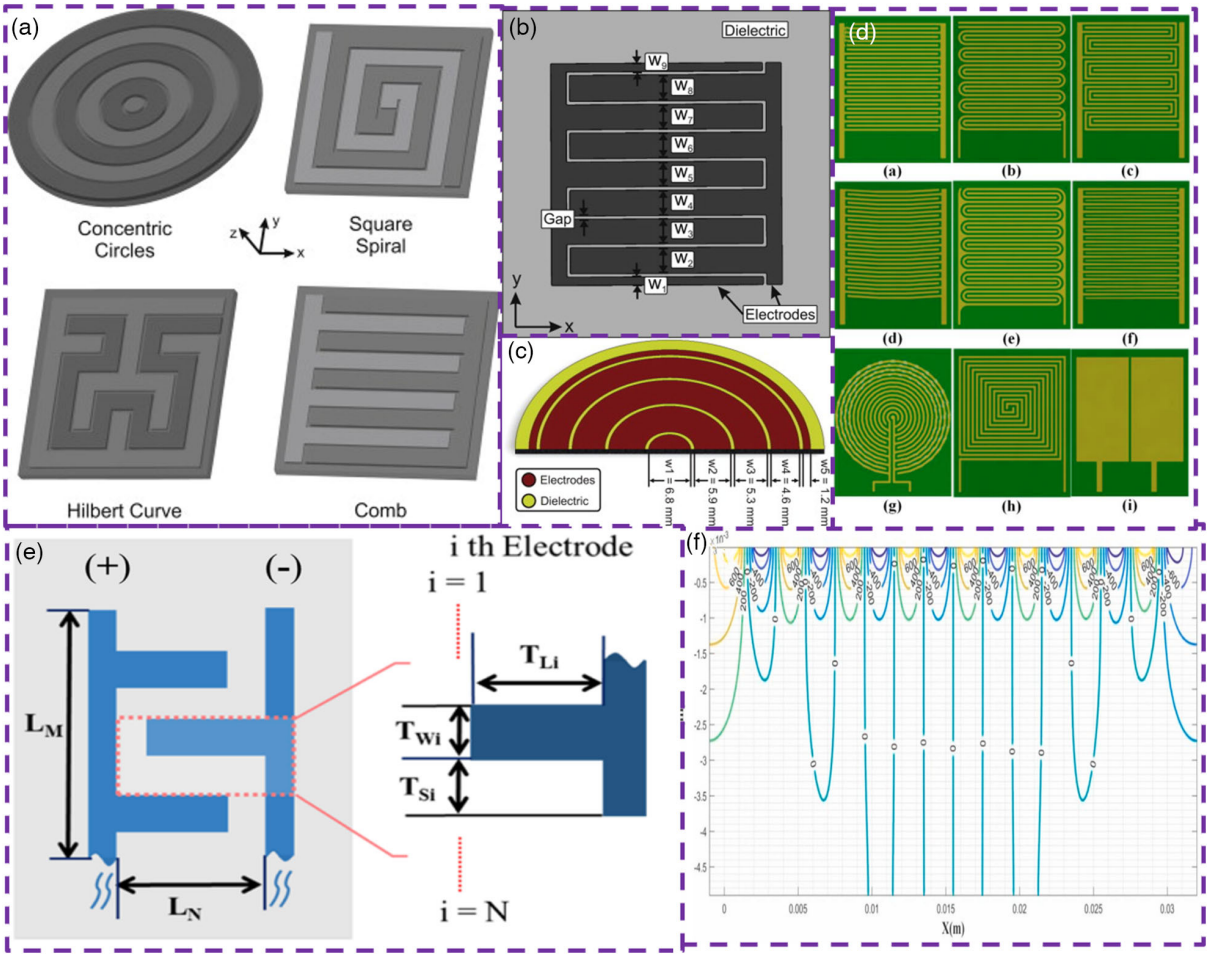

Figure 5. Theoretical and experimental investigations on the electrode geometry a) electrode patterns of interest for the theoretical investigations[61]; b–c) the pitch and patterns for IDT and concentric circular patterns. Reproduced with permission.[61] Copyright 2014, Elsevier; d) electrode patterns by Guo and co-workers. Reproduced with permission.[33] Copyright 2016, International Federation of Automatic Control. e) Dimension characteristics for the calculation of boundary edge ratio and electrode areal fraction for the force enhancement by Choi and coworkers. Reproduced with permission.[60] Copyright 2019, ACS; [https://pubs.acs.org/doi/10.1021/acsomega.9b00071 and further permissions related to the material excerpted should be directed to the ACS]; f) the capacitance can be measured using the conformal mapping technique in the FEM package by Masoud et al. Reproduced with permission.[65] Copyright 2021, Elsevier.

Figure 5a–c. The theoretical results were compared with the experimental evidence and showed that circular patterns performed the best due to the low leakage and absence of sharp corners. More advanced patterns shown in Figure 5d[33] indicated that circular design was not among the best designs as a variable-width method was not applied which reduced the overall area and thus the overall capacitance. However. in another design by Walter et al. spiral design was found to be better as compared to the straight tooth-based design[63] which was later reconfirmed by Dadkhah and co-workers as well.[64] It is important to note that the difference in adhesion between circular electrodes and parallel straight electrodes is subtle. Recently, Choi and co-workers looked into the geometry of electrodes on the localized charge distribution and interfacial polarization,[60] where the devices with different pitch (T_s) and electrode width (T_w) were fabricated and the forces were analyzed at different voltage conditions (see Figure 5e**)**. It is revealed that EA force was inversely proportional to the T_s and T_w. Electrode areal fraction (φ_A) which is the ratio of electrode area and the total area concluded a contradictory result. These suggested that T_s, T_w, and φ_A may not be the explicit geometrical governing factors for the EA force. From Equation (1), the equipotential field will be maximum at the smallest r value which corresponds to the boundary edges of the electrodes, where the boundary edge ratio (φ_B) is defined as $\varphi_B = \frac{\sum_{i=1}^{N}(T_{Wi}+T_{Si}+2T_{Li})}{2(L_M+L_N)}$.

This ratio aligned well with the assumption and the experimental observations. Hence, as the boundary edge ratio increased, the adhesion force simultaneously increased as correlated with the electrochemical impedance spectroscopy measurement. The impedance value changed for different materials which signify the polarizability of material affects areal adhesion force. Recently, Masoud et al. investigated the 2D and 3D geometrical electrodes using the ANSYS Maxwell platform using high-performance computing.[65] The capacitance can be measured using the conformal mapping technique, as shown in Figure 5f,

for 16 electrode pairs. As expected that at the smaller width of the electrode, the capacitance increases, thus increasing the overall force of adhesion. The patterns were tested in 3D settings as well where new patterns like sinusoidal patterns produced close to 70% higher capacitance compared to simple IDT patterns. The advances in electrode pattern design and fabrication have matured enough in the last few years which is improving the figure of merits of EA devices that will be reflected in the actual experiments. In the next section, we will throw some light on the advance in the material and fabrications aspects of cutting-edge EA devices.

3. Advances in Materials and Fabrication for EA Technology

As discussed earlier, the dielectric layer, the pair of electrodes, and the substrate are the most important components of the EA device. Here, we will discuss the advances in the dielectric film and electrode materials and their corresponding fabrication techniques.

3.1. Dielectric Materials

The insulating dielectric film is an important part of the EA device along with electrodes. **Table 2** compiles the key dielectric materials with the electrical and mechanical properties and the corresponding EA outputs. In this section, we will discuss the advances in dielectric materials and their role in EA.

3.1.1. Polymers

Semicrystalline polymers can have uneven structural polarizabilities, which is the primary cause of the EA effect.[3,66] The polymer can pick up insulating materials owing to the charge built on the surface when a voltage is applied. Various polymers have been used in the EA grippers or actuators such as Eco-flex, polyimide (PI), polyacrylate, polycarbonate, polyethylene terephthalate (PET), polydimethylsiloxane (PDMS), PVDF-TrFE-CFE, Parylene, and shape memory polymers.[67] Eco-flex is widely used for making EA pads due to its good stretchability and high stiffness, thus beneficial for the delicate handling of objects and picking up irregular objects. Germann et al. studied the influence of strain rate upon normal force and shear force of the stretchable EA pads.[68] The shear force (0.2–1.2 N) increased upon stretching due to the buckling effect. However, upon the stretching of EA pads, the normal force decreased, lowering the electric field and EA strength, resulting in the detachment of substrate and the EA pad. Similarly, Guo et al. developed electroadhesive integrated Eco-flex-based soft pneumatic grippers for pick-and-place applications.[69] This versatile gripper can lift

Table 2. Commonly used dielectric materials in the EA device and their corresponding parameters and electrical properties.

Material	Thickness [μm]	Voltage [kV]	Normal force	Shear force	Electrode	Approx. electric field strength [MV m^{-1}]	Approx. dielectric constant	Ref.
Eco-flex	2000	2	0.17–0.2 N	1–1.2 N	Carbon black	1.75	2.8	[68]
	200	4.8	–	10 N	Conductive silicon			[69]
	50	3	0.9 N	–	Carbon–silicone mix			[95]
Silicone	200	4	3.63 N	8.8 N	cPDMS	60	3.65	[71]
	100	5	0.7–1.3 N	3.5 N	Carbon			[59]
	200	4	4.11	12.78	cPDMS			[70]
Polyurethane	20	4.4	3.1 N	–	Copper	2	3.6	[75]
	20	20	123.4 Pa	–	Copper			[74]
	20	2	8.74 kPa	–	Copper			[72]
	20	2	33.1 kPa	–	Copper			[73]
Kapton polyimide	12.5	2	≈28 N	–	Copper	220	3.7	[5]
	10	5	–	≈5.1 kPa	Copper			[64]
	20	5	483 mN cm^{-2}	–	Carbon nanotube			[77]
VHB 4905	500	5	Lifted 5.2 g object	–	Conductive silicon	150	4.7	[81]
	≈31	5	–	3 N	Carbon			[82]
PVC	55	0.6–0.8	10^5 N m^{-2}	–	Copper	140–200	4	[79]
Parylene	0.7	0.04	4.5 N	≈90 kPa	cPDMS	220	3.15	[92]
	7	0.34	10.9 kPa	–	Copper			
PET	25	2	7 N	–	Copper	0.15–0.2	3–3.5	[85]
	130	5	–	48.68 kPa	Silver NP			[80]
PVDF	8	0.322	0.7 N	–	Gold	0.013	8.4	[83]
PDMS	70	3.5	16 N	–	cPDMS		2.4	[86]
	150	5	113.7 ± 36.2 mN	–	Conductive Ink			[97]
	68	9	–	11.86 kPa	cPDMS			[87]

irregular objects, including 2D shaped, complex, or nonplanar shaped, such as volleyball (80 g), the pulp (42 g), or extremely thin structures, plastic ID cards, porous cloth, and CD.

To improve its gripping behavior, Jun et al. fabricated a silicone elastomer-based soft gripper for a multifunctional polymer actuator.[59] The human finger mimicking device can be actuated by applying 3.5 kV across the membrane that generates opposite charges resulting in the electrostatic compression pressure along with the thickness and expansion in the planar direction. In addition, the gripper can pick miscellaneous geometries, such as a highly deformable water-filled thin membrane balloon (35.6 g), a raw egg (60.9 g), a flat sheet of paper (0.8 g), a Teflon tube (80.8 g), and a metallic can (82.1 g). Likewise, Chen et al. developed a silicone-based gripper for grasping high payload objects which can grip the object by adapting its shape. It could pick objects such as volleyball (262.6 g), a lamp bulb (166.6 g), and an irregular rock (125.6 g), the acrylic sphere ϕ300 mm (604 g), a water balloon (313.3 g), a piece of paper (23.3 g), and ID cards, as shown in **Figure 6**f.[70] The de-electroadhesion properties of silicone grippers from different substrate materials were also reported.[71,72] The release time is governed by the dielectric constant, mass-specific density of the object, compliance, molecular weight, and surface roughness, for example, the high dielectric constant materials take a longer time to release. **Figure 7**d schematic diagrams show the liquid metal electrodes embedded in the PDMS EA microchannel and other images show the stretchability of the device.

Choi et al. have examined an anionic waterborne polyurethane (WPU) as an insulating layer that was coated on copper patterned PI films. The polyurethane has high dielectric field strength and intrinsic polarizability which is the strategic feature for higher adhesive force and the corresponding device achieved a maximum force of 33.1 kPa at 1 kV, as shown in Figure 6c.[72,73] In addition, the PU gripper was demonstrated to grasp different objects, as shown in Figure 6e. Guo et al. examined the influence of different substrate materials with PU EA pads on the adhesion force.[74] Among them, glass (123.4 Pa) obtained a higher EA force than acrylic (46.3 Pa) and polycarbonate substrate (15.7 Pa). Texturing and surface roughness also influence the EA force; by reducing the root mean square height of the texture PI surface, the EA forces were increased from 1.7 to 3.1 N as explained earlier in Section 2.[75]

PI is often used for EA devices due to its commercial viability, high dielectric constant, high electric field strength, and

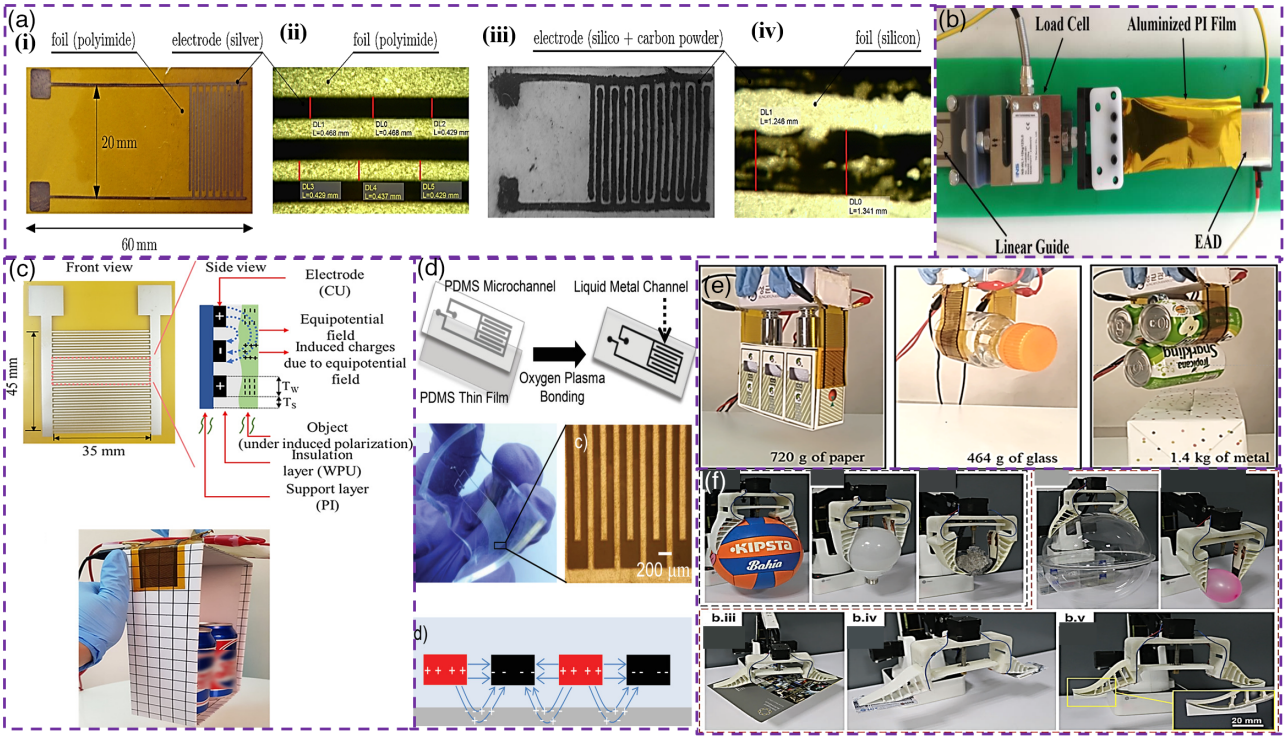

Figure 6. a(i)) The Interdigital silver electrode on PI sheet, (iii) electrode deposited on stretchable foil, and (ii and iv) microscopic image. Reproduced with permission.[95] Copyright 2018, The Authors. Published by De Gruyter. b) PEEK gripper tested with Aluminized PI film. Reproduced with permission.[84] Copyright 2020, SPIE. c) The Interdigital electrode with microgap and device demonstration; digital image of device grasping the paper box carrying two beverage cans. Reproduced with permission.[73] Copyright 2020, ACS. d) Schematic diagrams show the liquid metal electrodes embedded in PDMS electroadhesive microchannel and other images show the stretchability of the device. Reproduced with permission.[97] Copyright 2021, Wiley. e) Polyurethane gripper was Demonstrated to grasp different objects; paper box, glass bottle, and metal cans. Reproduced with permission.[60] Copyright 2019, ACS. [https://pubs.acs.org/doi/10.1021/acsomega.9b00071 and further permissions related to the material excerpted should be directed to the ACS]. f) Silicone gripper deployed to pick various object: a volleyball (262.6 g), a lamp bulb (166.6 g), and an irregular rock (125.6 g), an acrylic sphere with diameter of 300 mm (604 g), a deformable water balloon (313.3 g), a piece of paper (23.3 g), two ID cards (one weighting 6.1 g), and two customized ABS grooves (one weighting 5.2 g). Reproduced with permission.[70] Copyright 2019, Mary Ann Liebert, Inc.

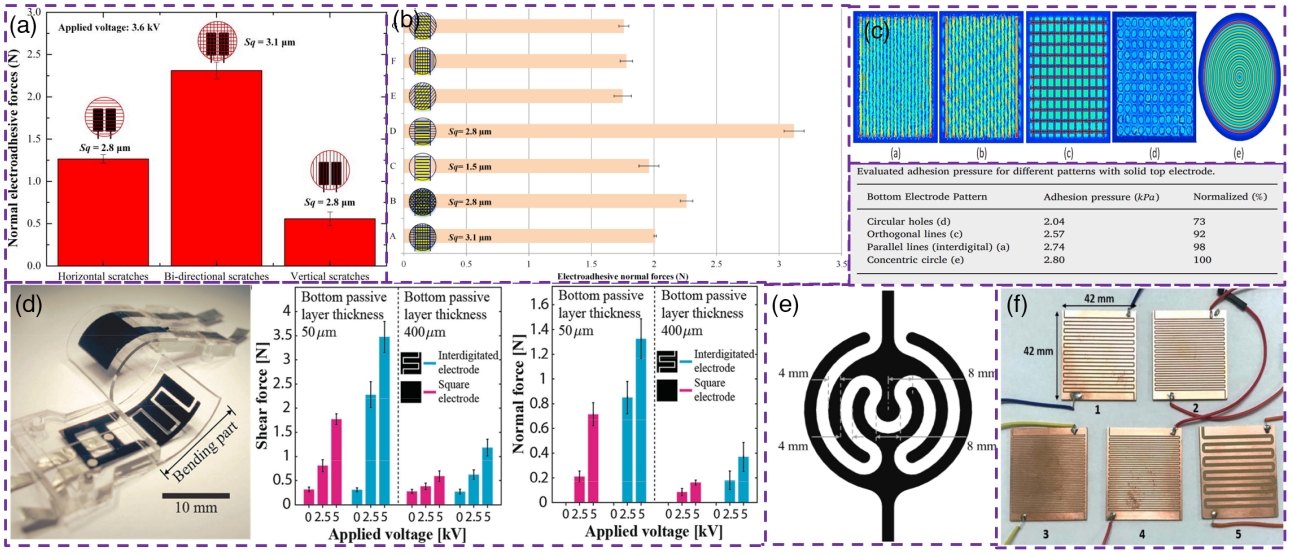

Figure 7. Comparison of normal EA force with different surface texturing on Al. Reproduced with permission.[74] Copyright 2017, AIP. b) Similarly, EA force analyzed with different surface scratches on Al (i) bidirectional, (ii) multidirectional, (iii) bare surface, (iv) horizontal, (v) scratched at 45° direction, (vi) vertical scratches, and (vii) scratched at 135°. Reproduced under the terms and conditions of the CC BY license.[75] Copyright 2016, The Authors. Published by IOP Publishing. c) Different structures of electrodes have been fabricated such as line pattern electrode, mesh or tiny square, circle, and concentric circle. Reproduced with permission.[64] Copyright 2018, Elsevier. d) Investigation of shear and normal force with two different electrodes surface by varying applied voltage from 0 to 5 kV. In that Interdigital electrode shows better performance. Reproduced with permission.[59] Copyright 2016, Wiley. e) A concentric-comb pattern with a diameter of 56 mm and width and gap of 4 mm. Reproduced under the terms and conditions of the CC BY license.[71] Copyright 2019, The Authors. Published by MDPI. f) CNC manufactured interdigital electrodes on the copper plate. Reproduced with permission.[180] Copyright 2020, IOP Publishing Ltd.

extraordinary environmental stability.[60,64,76–78] Hamza et al. modeled the Kapton-based gripper to attract metallic or polymer particles.[79] Compared to PVC particles, copper particles adhere considerably better at lower voltage due to the high mobility of free charge carriers in conductors. In conductive particles, charges align easily due to electrostatic induction, whereas in dielectric particles the dipole twisting is difficult to achieve. Berdozzi et al. used various dielectric layers for EA grippers such as PI, aluminized PI, inject printed PET, and coated PET.[80] Among them, aluminized PI had a higher dielectric field strength (236 MV m^{-1}), thus achieving maximum shear stress (48.68 kPa) and high capacitance.

Commercially available Very High Bonding tapes (VHB) are often used as dielectric elastomers for their high stretchability. Guo developed an EA composite gripper made of VHB4905 dielectric membranes, where the membrane is integrated with dielectric elastomer actuation (DEA) for sensing the internal deformation and dynamically morphing the curved surfaces.[81] These properties will be discussed in the following sections in detail. It was observed that EA–DEA composite gripper enhanced the sensitivity by increasing the number of coplanar electrodes and could pick and place the concave object of 23° of curvature and the contact area of 40 mm × 120 mm. Similarly, Digumarti et al. made an electrostatic adhesion-based multidirectional crawling robot using VHB with a maximum shear force of 3 N.[82]

Kai et al. designed a 2.5D refreshable high-resolution tactile display[83]; the actuated pins of the display can be electrostatically arrested to create the shape display. In this adhesive brakes, P(VDF-TrFE-CFE) tertiary polymer of 8 μm in thickness was used as the dielectric film coated with 50 nm gold interdigital electrodes. The high-density electrode with a 1.58 mm metal pin width attained a higher contact force of 76.3 gf (≈0.75 N). Berdozzi et al. used a polyether ether ketone (PEEK) dielectric layer with high dielectric strength (190 MV m^{-1}) for higher temperature applications, as shown in Figure 6b.[84] The EA device was demonstrated on the aluminized PI film that reaches maximum shear stress of 40 kPa at 7 kV. Chen et al. examined the effects of EA decoupling on miscellaneous configured EA pads[85] and realized excessive residual charge build-up and its influence on dipole moments in the pad dielectric cause an intensification in the depolarization of the electric field. This lowers the effective electric field and weakens the EA forces. Though usually, EA can easily lift materials higher than its original weight which reduces any extra efforts to eradicate the residual charges. However, for lighter materials, where residual charges create problem, researchers have proposed three different strategies: 1) natural discharge method, 2) high voltage resistor discharge method, and 3) field polarity reversal method.

On the other hand, the residual force can be useful in some circumstances; for instance, it can be used for slowly release of expansive and brittle parts which reduces the cracks formation during transport. It can be also useful in space technology which will avoid any distortions in the surface. The residual charges can be used in energy saving where smaller parts can be easily transferred without using extra energy. A PDMS gripper can even generate up to16 N lifting force, 1000 times greater than its original weight of 0.015 N.[86] A multilayered EA pad gripper made of PDMS generated shear stress of 12.41 kPa.[87] Sindersberger et al. constructed a magnetoactive polymer-based self-sensing

gripper to discharge the workpiece promptly. The gripper was fabricated by a magnetic particle-filled PDMS composite.[88] This gripper helps to separate promptly or increase the distance between the dielectric surface and workpiece by deforming the dielectric surface due to magnetic flux after deactivating the voltage supply.

3.1.2. Metal Oxides

Metal oxides are an interesting candidate for EA dielectric layers. Sanha et al. introduced a soft nanocomposite of Al_2O_3-coated carbon nanotube structures to manipulate the microscale objects.[89] A meager 0.2 nm thickness of Al_2O_3 has attained the high electrostatic attraction forces with a small voltage of 10 V. Lim et al. fabricated the gripper with 1–10 wt% of Al_2O_3 nanoparticle embedded PDMS matrix and found that 10 wt% composition attained a high force of 612 mN cm^{-2} which was twofold higher than the pristine PDMS gripper due to the high dielectric constant and field strength of the composite.[90] Vasudev et al. utilized the barium strontium titanate interfacial layers due to its high dielectric constant which is easy to polarize by applying high potential.[91] **Table 3** summarizes the advantages and disadvantages of metal oxides and polymers.

3.1.3. Low-Voltage Materials

Low voltage <1 kV is a key requirement for EA devices. One way of reducing the voltage is by decreasing the thickness of the dielectric film as it allows a high electric strength required for the EA devices. Parylene is an interesting material used in bioelectronics due to its high biocompatibility, high dielectric constant, inertness, and thin film deposition. Simpson et al. examined the critical shear force of conductive PDMS coated with Parylene dielectric film (0.38–1.4 μm) in low voltage conditions.[92] The maximum force of 4.5 MPa was developed with 700 nm thickness of dielectric thickness at voltage as low as 60 V. Xie et al. demonstrated a 7 μm-thick Parylene insulation pad for low voltage gripper applications with a strong lateral force (42–45 N) at 340 V.[93] Ionic elastomer is another option for lower voltage operation for EA devices.[94] An ionic polymer pair with oppositely charged layers could create a heterojunction at the interface. During the reverse bias, a molecular double layer forms at the interface which leads to high adhesion at voltage as low as 1 V. The interface is completely reversible and can be destroyed under the forward bias. These ionomers provide very high capacitance and force at a relatively lower voltage which makes them robust to dielectric breakdown and safer operation. Low voltage dielectrics is a new and active area of research for developing sustainable future robotics.

3.2. Electrodes and Fabrication

Typically, a pair of electrodes are covered with the dielectric medium in the EA gripper where a high voltage is applied to the electrode pair and an electric field is generated between them. The selection of electrode materials is vital to achieving high EA force, fast, and economical fabrication. Copper, aluminum, silver, gold, conductive carbon composites, graphene, and carbon nanotube are among the leading materials used as electrodes, as shown in Figure 7a–f.[68–75,77,80,83,84,95,96] Metallic electrodes have high conductivity and chemical inertness, but a highly reflective surface which makes them difficult to process via laser fabrication. Copper and aluminum are commonly employed as connectors or electrodes due to advances in Printed Circuit Board fabrication methods and affordability, though they are reactive and oxidize easily compared to gold and silver. However, the metallic thin films are not suitable for stretchable or very flexible substrates. Carbon composites are typical alternatives for stretchable electrodes. Conductive carbon nanoparticles such as carbon black, carbon nanotube, or graphene are mixed with soft polymers like PDMS for high stretchability and conductivity. Fessl et al. fabricated interdigital silver ink coating onto the Kapton PI and a carbon silicone composite-based electrodes for EA devices,[95] the latter produced superior adhesion force owing to its higher dielectric breakdown strength, as depicted in Figure 7a.

Fabrication methods also affect the cost, shape, size, and features of a device and can be classified as additive, subtractive, and hybrid manufacturing processes. For EA pad fabrication, additive manufacturing complies with a layer-by-layer approach or stacks the layers one over others following three steps: 1) bottom substrate layer, 2) electrode layer, and 3) electroadhesive dielectric layer. Similarly, hybrid manufacturing allows both additive and subtractive manufacturing processes in combination. Different methods of fabrication such as inkjet printer, blade-coating, casting, and spin or roll coating; laser ablation

Table 3. Advantages and disadvantages of the metal oxides and polymers which are commonly used in the EA.

	Advantages	Disadvantages
Metal oxide	Low residual forces	Brittle and rigid
	Lower chances of indentation	Expansive to coat thin films
	Possible to develop ultralow thickness	Poor scalability
	Higher electric breakdown	May not be suitable for high humidity environment
Polymers	Low cost	Shorter life span
	High flexibility	High residual forces
	Scalability	Lower damage tolerance
	Environmentally inert	Lower electric breakdown

Table 4. Conventional and advanced fabrication method for EA pads and electrodes.

	Methods	Layer	Advantage	Disadvantage	Ref.
	Inkjet printer	Both dielectric and electrode	Write on the flexible substrate and less material wastage	Being sluggish, expensive	[74,80,84,95]
	Blade coating		Scale fast and large area deposition	Governing thickness is difficult	[59,70,85–87]
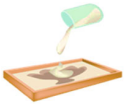	Casting	Dielectric	Multilayer coating, low fabrication	Superficial surface finished mold required	[64,72,82,92]
	Spin coating		Fast-drying, deposit various thicknesses with great consistency	Difficult to deposit low viscous material	[97]
	Laser scribing or cutting	Both dielectric and electrode	Fast process, easy scaling (macro to nano)	Can contaminate	[69,81,83,87]
	Machining		Mass production	Not suitable for flexible materials	[83,180]
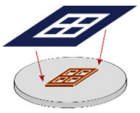	Photolithography		High precision, intricate part fabrication	Expensive requires a sophisticated environment	[60,73]

and cutting, chemical etching, and photolithography are compared in **Table 4**. Inkjet printing enables the direct writing of electronics onto flexible substrate materials[74,80,84,95] via a dropwise and noncontact process that selectively deposits a wide range of materials onto different substrates. The process provides flexibility in the electrode design and can be readily printed with lower material wastage. However, it is confined to a tiny subset of materials and also slow, expensive, and inappropriate in mass manufacturing. Casting is the easiest method for the fabrication of multiple layers.[64,72,92] Krishna et al. used a mask instead of an engraved mold to improve the EA design,[82] but it was limited to viscous materials. Blade coating is an industrial scale, fast, large area, and economical coating process for both dielectric layer and conductive electrode tracks.[59,70,85–87] However, controlling the thickness in submicrometer zones is challenging due to the complex properties at the solid–liquid interphase during curing. Like blade coating, spin-coating is also limited to viscous materials, and is often not suitable for large area deposition, but can reprduce material thickness with fast drying that is essential to scale up the device production with high consistency.[97] EA force is typically dependent on the shape or pattern of the electrodes as discussed in Section 2. Patterned electrodes have been fabricated by advanced processes including etching and photolithography,[60,73] although these processes are expensive and require controlled conditions. There is a demand for more precise and tailored EA pad manufacturing solutions that are cost-effective and efficient in mass production. Thus, laser scribing or cutting and the conventional machining process have proven to be facile, repeatable, and accurate methods for designing the electrode pattern and bonding to the dielectric layers,[69,81,83,87] although they involve manual handling for bonding the dielectric layers.

4. Extensive Applications of EA

EA technology is versatile encompassing futuristic growth areas such as robotics, optoelectronics, tactile displays, haptics, biomedical, and space applications. The recent advances in robotics, functional polymers, and fabrication methods have opened new pathways for EA technology. Driven by automation and robotic assembly at large-scale manufacturing, there is an urgent demand for high-performance EA technology, which holds the potential for commercial viability. The key applications and their subsequent parameters are highlighted in **Table 5**.

Robotic grippers play an important role in industrial automation which improves the manufacturing speed, efficacy, cleanliness,[7] repeatabilities, safety, and continuity of operations.[98] One simple application of the EA is that of an effector for prehension where the material is picked and placed to the location of interest. Guo et al. defined the end effectors

Table 5. Key applications and the strategic device parameters of the EA devices.

Sr. no.	Application	EA parameters	Dimensions [cm]	Force/pressure/torque
1.	Prehension of pads for telephonic relay applications[2]	440 V DC supply	81 cm^2	–
2.	Clutch for stopping rotating cylinder[11]	150–300 V; 30 mA	Dia. 6.3, height 1.9	≈3.4 Nm (torque)
3.	Prehension for space application[14]	6 kV; 0.05 mA	26.2 cm^3	≈9.1 N cm^{-2}
4.	Electro tactile display[25]	Rectangular biphasic pulse of >50 V	Area≈16 cm^2 with equal spaced protruding needles	N/A
5.	Prehension in textile[20]	–	≈100 cm^2 (approx.)	0.005–0.14 N cm^{-2} (strength is different for different materials)
6.	Chuck for wafer handling[62]	0.5–3.5 kV	100 cm^2	Drag force <50 N
7.	Microgripper using capillary action of liquid[91]	8–28 V	Dia. 0.2 cm	213 μN
8.	Prehension and wall climbing robots[109]	4 kV DC	40 cm^2	Lateral 0.08–1.4 N cm^{-2} Normal 0.2–4.2 N cm^{-2}
9.	Electrodry hybrid EA gecko adhesion (GA)[169]	0–4 kV	43.5 cm^2	Shear bond strength 0.5 N cm^{-2}
10.	Satellite repair robot gripper (EA/GA hybrid gripper)[76]	3 kV	50 cm^2	3.5–45 N
11.	Gripper for handling fragile soft parts[59]	2.5 kV	EA area 1 cm^2	3.5 N
12.	High payload gripper[77]	6 kV	100 cm^2	0.8 N cm^{-2}
13.	Shape inspired soft-robotic gripper[70]	4 kV	8.8 cm^2	12 N
14.	Soft wall-climbing robots[153]	5 kV	8 cm^2	0.9 N (tangential) 0.15 (normal)
15.	Ultrasoft and light weight robots[181]	3 kV	22.8 cm^2	0.11 N
16.	Stretchable EA for soft robots[68]	2 kV	4 cm^2	Detachment force 1.8 N Shear force 1.3 N
17.	Large-area electroactuator for end effector applications[182]	0–15 kV	≈350 cm^2	1–110 N
18.	Perching robot[117]	1 kV	0.63 cm^2	0.0025–0.02 N cm^{-2}
19.	Multidirectional crawling robot[82]	2–5 kV	$\Phi = 6.3 \times 3$	0.5–3 N
20.	Very thin low voltage EA devices[92]	60 V	0.5 cm^2	Critical shear force = 7 N

based on structural deformation capabilities into rigid, flexible, and stretchable devices.[8] However, these can be further classified based on the skills like simple prehension devices, self-sustaining devices, smart and sensitive devices, hybrid EA-gecko devices, or hybrid electro-actuated devices. In the simple pick-and-drop applications, Kyoko and co-workers utilized the EA technology for handling the 4 inch silicon wafer for the vacuum environment.[99] Here, a sealant was added to the wafer to remove air gaps which tend to cause the dielectric breakdown.[99,100] The system was later developed to be used in a vacuum as well as using a thin ceramic layer along with sealant.[101] Researchers also utilized the hairy patterns to enhance the adhesion strength through biomimicking the gecko feet (discussed in detail in Section 6).[102–104] Sun et al. fabricated the chucks suitable in a vacuum etching environment like reactive ion etching.[105] Kesheng et al. worked on the theoretical and experimental investigations of the residual charges in the electrostatic chuck which increase the decoupling time in the batch process and increase uncertainty in the declamping process.[7] EA is an interesting technology for the semiconductor industry. Besides simple pick-and-drop applications, the EA has been used in a variety of other applications for instance handling of textile fiber, prepregs in composite shop, and textile industries.[3,20,106] These systems can help in the robotic layup process in the hazardous environment of composite handling. They can also help in the automatic folding of clothes in textile industries, showrooms, and warehouses. Over the years several patents were filed in the semiconductor wafer handling system. Recently, a patent was filled incorporating this technology in gripper shoes which are paramount in hiking and mountain climbing expeditions to improve the grip.[107]

EA has also been implemented in the wall/vertical climbing robots due to quieter operations, applicability on a variety of surfaces with low power requirements. They are suitable for urban reconnaissance, search and rescue operations, military operations, and sensor deployment. Akio et al. used the flexible monopolar electrodes on a flexible PI surface.[108] Prahlad et al. at SRI International fabricated a few wall climbing robots with bipolar electrodes and tested them on various construction materials like wood, concrete, brick, glass, or metal.[109] They successfully demonstrated the tracked tank and inchworm-type robots. Chen et al. fabricated a double-track wall-climbing robot

that can climb up and down and even can turn on a slightly slanted surface.[110] Mao et al. worked on the simulation and modeling of the EA-based wall climbing robots using ANSYS.[111] Keng et al. improvised the previous design and biomimic the gecko tail functions to optimize the center of gravity, as shown in **Figure 8**a,b.[112] The hybrid EA device works for adhesion and actuation due to the presence of dielectric elastomer actuation. The detailed evaluations of dielectric actuation with EA will be discussed in the subsequent sections. Rong and co-workers fabricated a similar wall-climbing robot with tracked Kapton electrodes and a tail, as shown in Figure 8c.[113] Wu et al. fabricated a shape memory alloy (SMA) and EA hybrid robot made of paper.[114] A star-shaped design with EA pads on each corner is connected by SMA wire diagonally. The change in actuation of wire and alternating adhesion can result in vertical and horizontal moments.

EA technology was also used in space-related applications such as satellite repair robots, gripping applications in space stations, and debris collectors. The devices are suitable to be used in low vacuum, wide range of temperature, and radiation active environment with relative ease compared to other methods. Moreover, its low energy requirements and residue-free adhesion make it an interesting choice for such applications. Braven et al. tested the docking characteristics using the monopolar electrodes, where the device was tested on the surface with a frictionless spherical bearing base for calculating the normal, shear, peeling, and twisting forces. The test was conducted in a pure air atmosphere as well as in the vacuum environment at NASA Marshall Space Flight Center.[115] The team reached new heights when they reported their findings aboard NASA's C9B zero-gravity airplane in two missions.[116] The hybrid gecko devices with motor and EA are used as satellite repair robots[76] which can be modified for space debris capture as well.[63] The technology was also demonstrated in the flying robot to dock and perch in a controlled flight which might be suitable applications in repair robots, reconnaissance missions, and military applications and are shown in Figure 8d.[117] The technology holds a promising future for handling critical bulky mechanical parts without causing deformations like wind turbine blades and composite panels.

These devices have been used in medical fields as well where, recently, Leah and co-workers used a polyelectrolytic gel to heal the animal tissue puncture.[118] Under a 10 V DC field, the materials adhere to each other and due to the polyelectrolytic interface,

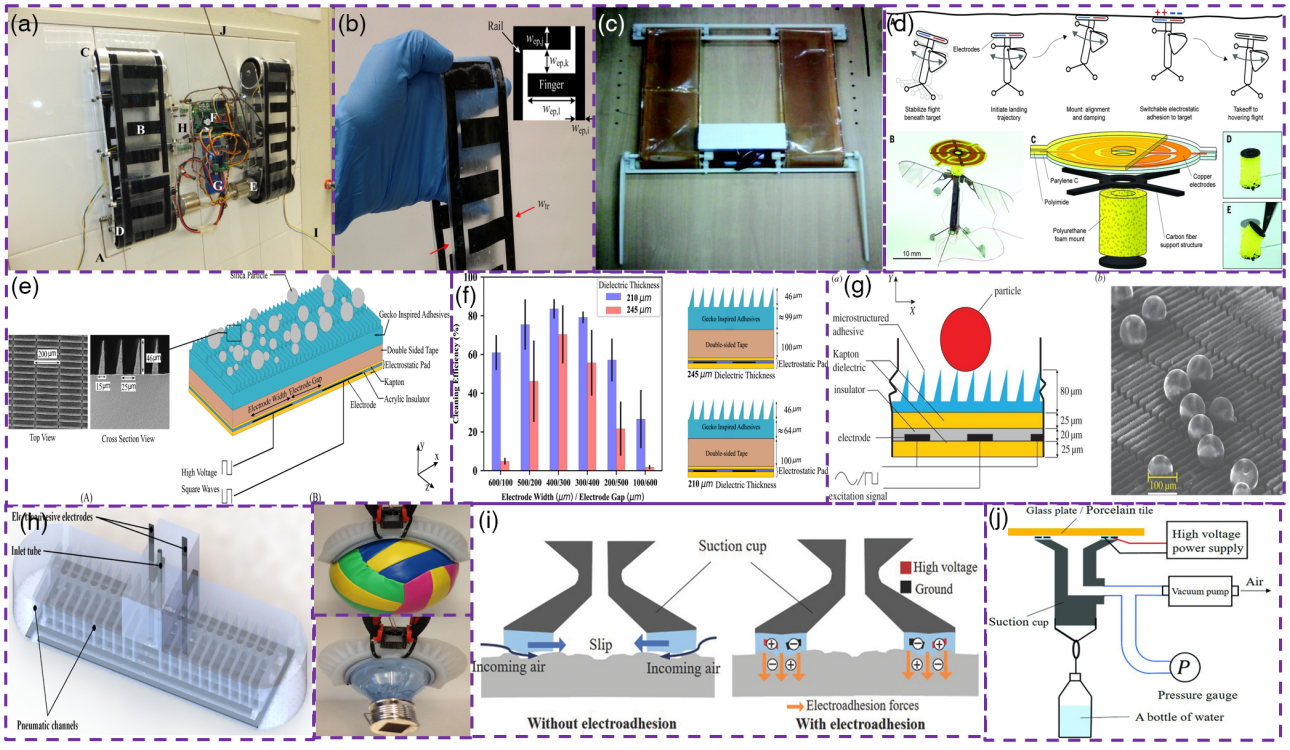

Figure 8. General application of EA devices (a–d) wall climbing or perching robots; a–c) a large-scale vertical wall climbing biomimicking robot trying to retain the center of gravity as close to the surface to avoid detachment from the wall similar to gecko; the device even demonstrated the use of tail to do similar things. a,b) Reproduced with permission.[112] Copyright 2016, Elsevier. c) Reproduced under the terms and conditions of the CC BY license.[113] Copyright 2013, SAGE Publications Inc. d) The design and flight of the flying robot with an EA surface embedded on the top facilitating the perching on the ceiling. Reproduced with permission.[117] Copyright 2017, AAAS. e–g) Dust trapping EA devices: (e) the design of gecko-inspired hybrid EA device for dust trapping; (f) the cleaning efficiency of the device with different electrode pitch width and dielectric thickness. Reproduced with permission.[121] Copyright 2020, Elsevier; (g) the schematic of dust trapped on the surface and the corresponding SEM image for the same. Reproduced with permission.[122] Copyright 2018, The Royal Society. h–j) The pneumatic gecko based hybrid devices: (h) the design of pneumatically actuated EA device where pressurized air deforms the shape of gripper and stretchable EA helps in adhering very soft and delicate objects; inset shows the griping of a soft ball and glass bulb[69], Creative Commons Attribution License 3.0; (i,j) the design of vacuum gripper which improves the griping and life of pneumatic technology. Reproduced with permission.[124] Copyright 2018, Wiley.

the bond remains permanent even after the removal of electric voltage. However, the bond is electrically reversible and can be deadhered using the reverse polarity at the interface. This provides an interesting and unique approach in biological fields. Previously, the technology was also demonstrated to be used in vitreoretinal surgery protocol by carefully handling live tissues using EA.[119] In such complex surgeries, the separation of membrane tissues is usually handled by microtweezers which often ruptures the tissue during the gripping phase. For the minimalistic postsurgery trauma, EA was demonstrated to be an ideal technology. Due to intimate contact, the electric pulse was supplied only once to adhere the tissue to a gold electrode. To reduce any damage arising due to electrical signals, the frequency, amplitude, and polarity of the signal were optimized which might further improve the healing.[57] The electrostatic clutch is also an interesting technology that utilizes the principles of EA for arresting, holding, and brake applications.[120] In recent years, renewable energy, especially solar cells, is competing to become the chief source of energy. However, the dust which gathers on the surface remains the bottleneck of the real-life performance. Vahid and co-workers have developed a hybrid EA device for dust removal applications.[121–123] The process, design, and mechanism were studied in great detail to maximize the cleaning efficiency. Here, the voltage and electrode patterns pitch was optimized. The Gecko-based hybrid device approach was utilized in this research as it was seen from previous experiments that these patterned surfaces were quite good at adhering the dust particles. Repulsion, sliding, and rolling were identified as three possible mechanisms of which the repulsion was of least importance. Figure 8e–g shows the schematic and cleaning efficiency of the device. The technology has demonstrated the potential for microparticle collection and holds a promising future in attracting/collecting or separating nanoparticles in an assay. The technology has been implemented in the Opto-mechatronics research field as well and is used as a varifocal lens and microfluidic application and will be described in Section 5 and 6.

Hybrid devices coutilizing EA along with pneumatic action could improve the overall efficacy of the pneumatic system. Guo utilized the soft pneumatic robotic gripper with stretchable EA electrodes.[69] A hollow cavity inside the stretchable surrounding can be deformed by air pressure which makes an interesting choice as a two-jaw gripper along with EA capability. Figure 8h shows the design and applications of the hybrid device along with the gripping of soft and delicate objects. Yuto et al. employed an EA device in the face of a vacuum gripper to reduce the gap between the substance and gripper, as shown in Figure 8i, j.[124] EA improved the gripping and suction performance over both rough and smooth objects. This simple addition increases the lifetime of the attached vacuum pump and suction gripper. This technology was also demonstrated in the paper turning machine as well which can be potentially used in fully automatic copier machines.[125] EA technology has also been employed in responsive tactile displays for visually impaired people as well.[83,126] Shultz et al. exploited 6061 anodized aluminum for EA behavior for such applications.[127] The combination of high resistance epidermis and very low current output from the Trek current amplifiers makes it more convenient to use the bare metal plate. A total voltage of 800 V was supplied across an 8-Mohm load resistance to activate the EA characteristics, with a direct current of 100 μA and it demonstrated to adhere on the human skin. It was observed that the electroadhesive property is very strong and stabilizes at the electrostatic normal force of 7 N. These were some general application areas and in the next sections, we will discuss some specialized segments of EA.

5. Independent and Smart EA Devices and Their Applications

5.1. Triboelectric Nanogenerator Powered EA and Inter-Related Applications

Triboelectricity is a form of transducer application where mechanical energy is converted into electrical energy by virtue of contact electrification and electrostatic induction.[128] When two materials (usually insulators) with different surface potential comes in contact, the surface potential reaches an equilibrium state. This pushes a few electrons out of the circuit, thus producing electricity.[129] When surface departs, individual surfaces try to restore the initial surface potential balance, hence the transferred electrons rush back to individual materials via an external circuit. The technique has been known for centuries however, recently received huge attention from the research community owing to its increased research in low power electronics, the internet of things, and wearable devices.[130,131] **Figure 9**a shows the mechanism of charge transfer during a contact-separation mode of the electrification cycle. There are other modes of energy transfer for triboelectric nanogenerator (TENG) and it shows many interesting properties as well which readers can read from here.[132] Due to the high impedance of devices, they often produce very high voltages and have been shown to produce few kilovolts (kV) with a current value limited to a few microamperes (μA). They are recently shown to power interesting applications like biomechanics monitoring, VOC sensor, accelerometer, and even high voltage applications like electrospinning and mass spectroscopy.[132] The high voltage property and low current are direct gateways to be implemented in EA and related technologies. Wang's group utilized this approach to implement TENG in a variety of EA applications and will be discussed in this section. This technique removes the need for bulky batteries and high-frequency amplifiers and simplifies the existing experiments.

Xu et al. used the TENG for EA technology by increasing the voltage by more than tenfold employing a unique charge supplement strategy.[133] Initially, the EA device dielectric layer with different materials was tested and optimized using an external power supply. For TENG, aluminum foil and Teflon (PTFE) pair were chosen as the positive and negative triboelectrics material which show the high surface potential difference. Multiple units were combined to form a high output integrated unit and an EA device was mounted on the surface as shown in Figure 9b. Without a high voltage diode, the output from TENG was limited to 200–300 V which was not sufficient to drive the EA device; however, after employing diode the output reached as high as 3 kV. This voltage was sufficient to lift heavier objects. Moreover, they integrated a high voltage capacitor and made

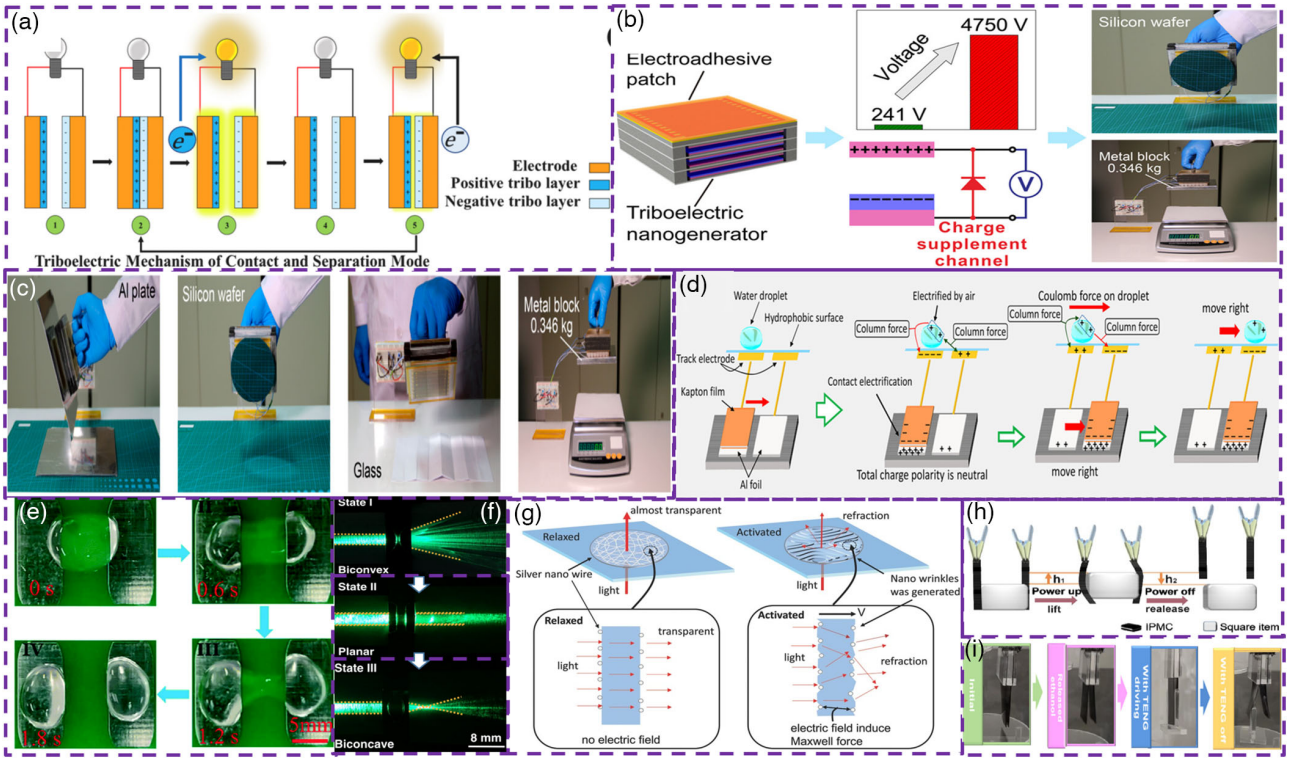

Figure 9. TENG powered EA and hybrid EA devices. a) Principle of charge transfer in the contact separation mode TENG; when two materials (usually insulators) with different surface potential come in contact with each other, the surface potential reaches an equilibrium state and pushes few electrons out of the circuit, thus producing electricity. When surface departs, individual surfaces try to restore the initial surface potential balance, hence the transferred electrons rush back to individual materials via electron circuit. Reproduced with permission.[131] Copyright 2020, Elsevier. b–c) A multilayered triboelectric device using the charge supplement diode to enhance the output. This demonstrates the adhesion of various materials like Al plate, silicon, glass, or metal block using the electricity produced by TENG. Reproduced with permission.[133] Copyright 2018, ACS; d) Working principle of the self-powered microfluidic transport system for two electrodes. Reproduced with permission.[134] Copyright 2018, ACS; e) demonstration of splitting of the droplet of 0.4 mL under the TENG electrical force. Reproduced with permission.[137] Copyright 2020, RSC; f) demonstration of a laser beam modulated by the TENG powered varifocal lens. Reproduced under the terms and conditions of the CC BY license.[139] Copyright 2020, The Authors. Published by Springer Nature; g) the schematic of the working principle of a smart optical modulator, where silver nanowires can generate nanowrinkles to change the transmittance powered by TENG source. Reproduced with permission.[140] Copyright 2017, Wiley; h) ionic polymer–metal composites schematic for lifting the weight using actuation produced by TENG. Reproduced with permission.[143] Copyright 2019, ACS; i) a simple electrostatic actuator lifting a slab of PDMS powered by TENG. Reproduced with permission.[142] Copyright 2019, Elsevier.

handheld devices as shown by Chrysler space division (Figure 2), however without an external battery. The device was even mounted upon a robotic arm to work as a pick-and-drop system in the industry. A variety of things were experimented for the adhesion test like metal block, aluminum plate, glass, and a silicon wafer, as shown in Figure 9c. These results show the possibility of integrating TENG with high voltage low current applications like EA.

Besides, TENG has been employed in a similar high voltage application which is partially related to EA and we will mention it here in brief. Dielectrophoresis is an electrostatic technique used to move liquids on the surface of the hydrophobic dielectric layer by application of high voltage. This effect is a quite similar EA involving fluid in place of solid on a hydrophobic surface, where high potential allows the moment of fluids. The detailed relationship will be discussed in Section 6. Nie et al. used the TENG and EA for the manipulation of simple water droplets using the sliding mode TENG.[134] In the sliding mode TENG, Kapton, and aluminum foil were used as triboelectric layers which produced very high voltage. As the Kapton slid on the tribopositive layer which was connected to the roller pattern, the droplet was attracted to the electrode and moved as the triboelectric layer moved. The mechanism of locomotion is shown in Figure 9d. The drop was capable of even carrying the external weight (500 mg) along with the self-weight and was able to traverse large distances. A variety of experiments were performed like the maximum distance and volume for the efficient transfer. A similar experiment with different liquids and even solid steel balls was performed by Zheng et al. and Nie and co-workers.[135] With the optimized conditions, the drops could be moved as far as 20 mm. A model was proposed in the experiment involving the influence of surface hydrophobicity on the motion of droplets. However, the distance of travel remains poor for the droplet due to poor contact angels between the surface and droplet. To encompass this problem, they worked out to use a photocontrollable adhesion surface using semiconductor coating (titanium dioxide and UV light treatment).[136] This increased the contact angle and the droplet could travel as large as 640 mm. The voltage was sufficient to work

for thicker dielectrics as large as 2 mm. The work also demonstrated to manipulate drops across the liquid interface to show the possibilities of controlled chemical reactions/mixing. Recently, a prototype for enhanced functional droplet manipulation, mixing, splitting, merging, etc. was demonstrated by Yu et al. using a rotary triboelectric device.[137] Figure 9e shows the splitting of the droplet of 0.4 mL under the TENG electrical force. Apart from insulating liquids, conducting liquid metal droplets can also be moved using this technique which follows the adhesion principle shown similar to Figure 1.[138]

Electrowetting (EW) is a similar technique used to manipulate the contact angle of drops with the substrate using high voltage but does not necessarily involve movement. Fanget al. used this technique to vary the shape of clear liquid polymer and used it as a varifocal lens.[139] Here, the poly-phenyl-methyl-siloxane polymer was used as the optical material which has a high viscosity and 90% visible radiation transmission. Using a free-standing mode of tribo using textured FEP and copper films, the voltage output was as high as 7 kV which was sufficient enough to modulate the shape of the polymer at the liquid–air interface. Figure 9f shows the diffraction of light employing the TENG-controlled varifocal lens.

Electroactive elastomers can demonstrate larger strain when initiated by an external electric field. Chen and co-workers used dielectric elastomers in conjunction with TENG for the optical modulator applications.[140] Here, the acrylic polymer was pre-stretched and coated with transparent Ag nanowires and connected with a carbon grease-coated elastomer in series. When the device was coupled with a single electrode mode TENG, it could produce nanowrinkles on the surface due to electroactive deformation under electric field, as shown in Figure 9g. This deformation eventually reduced the transmittance of visible deformation and the material turned from transparent to opaque owing to the distortions in the path of light through the material. The system was later developed for the modulation of optical gratings and was powered by a similar TENG device.[141] Apart from microscopic deformations used to diffract light, similar applications can be used for lifting heavier objects by actuating larger distances similar to EA but with much lower energy requirements. Zheng et al. showed both surface mediation (wrinkle formation) as well as full-scale actuation using TENG.[142] Figure 9h,i shows the actuation of polymers used for lifting devices like EA and shows promising prospects for applications in underwater robotic and navigation applications. Yang et al. fabricated an ionic polymer composite with metallic particles embedded in the surface with a carbon nanotube electrode.[143] It is interesting to note that the device achieves 42° deflection with 150 μC charges supplied by TENG whereas it took 500 mC from a DC power supply to reach a similar deformation, demonstrating that TENG produced a better electrostatic field compared to an external battery. This reiterates the fact that TENG can be a potential technology in futuristic EA devices.

5.2. Smart and Sensitive EA Devices (Exteroceptive/Proprioceptive)

EA devices have received increasing attention due to their highly anticipated commercial and industrial applicability. Its commercial success largely depends upon its energy efficiency, prehension forces, wide surface selectivity, ability to withstand harsh environmental situations, more importantly, and reliability. In complex environments such as a space station where the device needs to handle multiple objects at different voltage conditions, therefore, there is a need for a feedback system to constantly monitor the surface characteristics of the device to ensure reliability. The feedback system can inform the control unit to increase or decrease the system voltage which will allow reliable and safer operations.

Guo et al. found that the EA normal force is largely dependent on environmental factors like temperature and relative humidity.[144] This leads to different adhesion forces generated under the same electric field which must be taken into consideration for automatic and independent systems. Hence, using a LabVIEW programming a protocol for an independent system could take feedback from different integrated sensors. Here, a force sensor will monitor the initial force when the EA pad contacts the surface, coupled with a humidity sensor and temperature sensor for environmental monitoring. A capacitive sensor was also mounted which was used to identify the conformity and material identification. The capacitance values for different materials are already fed into the system which recognizes materials based on interfacial capacitance values. This property of the device to identify the prehension material and change the strategy is known as the exteroceptive property of the device. This entire data is fed into the system which then controls the high voltage supply and the motor to control the position, velocity, and time of the contact of EA pads. The feedback system ensures the smooth working and reliability of operations. However, a truly intelligent device will be the one with not only exteroceptive property but also the proprioceptive property. In the proprioceptive property, the device can sense the internal changes such as deformations and strains in itself and provide feedback to the control system about such changes to alter the adhesion controlling parameters as per the need. Guo et al. fabricated an intelligent EA device having proprioceptive ability.[81] Here, when the voltage is applied, the flexible device deforms much like an electroactive actuator due to intrinsic flexibility and Maxwell force between the electrodes. Once the conformal contact is achieved as shown in **Figure 10**a, the capacitance of the system changes due to local deformations and the controlling system can be notified about the material and little information about the extent of deformation. The already trained system then can apply the required voltage to complete the task. The system can be tailored to know the shape of the sample by using a visual-tactile system.[145] In this system, stretchable arms hover over the surface of the material; a mounted camera predicts the shape of the structure using image processing. This allows the system to inhale or inflate by the attached pneumatic system, as shown in Figure 10b. Moreover, with the visual system, the control system identifies the approximate area which helps the system to decide the optimum voltage values require to reliably complete the task. A similar feedback system using a simple load cell was used in the hybrid pneumatic design where pressurized air deforms the shape of the gripper and stretchable EA helps in adhering to very soft and delicate objects.[69] The start of pneumatic and EA actuation was controlled by the load cell and touch-based feedback system, as shown in Figure 10c,d. Walter and

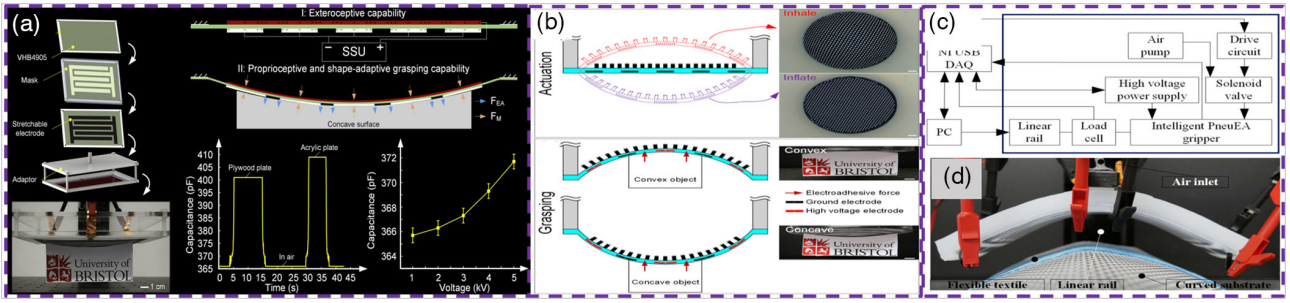

Figure 10. Intelligent EA devices. a) The fabrication steps involved and the demonstration of Exteroceptive and proprioceptive abilities and the corresponding characterization curves. Reproduced under the terms and conditions of the CC BY license.[81] Copyright 2018, The Authors. Published by Elsevier; b) shape adaptive pneumatic EA device Reproduced under the terms and conditions of the CC BY license.[145] Copyright 2019, The Authors. Published by IOP Publishing; c,d) intelligent pneumatic-based hybrid EA system flow chart and actual device. Reproduced under the terms and conditions of the CC BY license.[69] Copyright 2018, The Authors. Published by IOP Publishing.

Bogdan designed an advanced EA device that contained a series of strain gauges and piezoelectric composite structure along with an EA device.[63] The device was fabricated for little or no curvature/roughness knowledge of the surface and can be used for space debris capture. Based on the strain gauge reading, the device will be actuated by the piezoelectric actuator. With the help of feedback signals, sequential sensing, and actuation, the shape of the device will be adjusted which results in improved adhesion. These intelligent systems are still in the early stages of development and will witness further improvements in the years to come.[146]

6. Hybrid EA Technology

6.1. Electroactive Polymers and EA Hybrid Devices

Electroactive polymers are a class of polymers where the deformation/actuation can be performed using an electric field or ion-concentration gradient.[147,148] The electronic or field-assisted actuators[149] are activated by the coulombic interaction between the electrodes when the voltage of alternating polarity is applied to the device. This is quite similar to EA technology, however, in electroactive polymers, the electrodes can be of the sandwich-type as well as planer (interdigitated electrodes) whereas in EA devices it is almost always planer (recently some new designs are an exception to this[59]). Usually, the applied voltage is near the dielectric breakdown range of these polymers due to the lower dielectric permittivity of these materials. Moreover, the actuation is low in this case that is why many researchers use the multiple stacking of layers similar to piezoelectric actuator stacking or use flexible and elastic soft materials (dielectric elastomers). In contrast, the ionic actuators require two electrodes and an electrolyte and work on the principle of ionic species diffusion at the electrolyte electrode interface.[150] Hence, they either require wet (aqueous electrolyte) or solid electrolyte to perform the required task. They actuate large strain values at relatively low voltages (0–10 V) and are very useful for low power actuation applications. However, they are relatively slow coupling and decoupling applications.

Hence, the synergistic effects of polymer actuation and conformal adhesion can be a very efficient system for applications like grabbing, lifting, actuating, and plucking. Moreover, it can be easily speculated that flexible adhesion film will impart a higher surface area of contact for nonflat surfaces compared to stiff films. Besides, the conformity will improve the adhesion force compared to involving individual procedures. This will also result in the reduced consumption of energy and improved safety standards. However, the majority of these actuators are used in a variety of soft robotic applications and there are separate review articles on the electroactive polymers for soft robotic applications which readers can find very interesting to read.[147,149,151] Here, in this section, we will discuss the electroactive polymers in reference to EA without deviation from the main topic.

Shintake et al. fabricated a versatile gripper involving both EA and electroactive polymer techniques for the robotic gripping of very delicate objects.[59] Here, a pair of the prestrained elastomeric membrane was put in between the complementary electrodes, and voltage was supplied. It was observed that this unique design improved the adhesion force by tenfold compared to conventional electroactive elastomeric devices. Besides, the device architecture was designed for synergistic use of both electroactive polymer and EA simultaneously. The IDT device electrode architecture was experimented with and was compared with the square electrode parameters to check the forces acting on the load cell. The clutching was fast and the gripper was able to lift a variety of materials, as shown in **Figure 11**a–c. The new architecture could lift things more than 50 times (85 g) its weight (1.5 g) and can handle delicate objects. Electrode design was further modified to improve the force of adhesion.[86] Bin and Xinyu recently utilized a similar sandwich pattern electrodes for handling the fabric.[152] The three-layered, four flat padded robotic arms were using EA and slider-crank mechanism to flatten the wrinkled fabric and be implemented in industrial settings. Guoying and co-workers employed the electroactive polymer for actuation and EA for the locomotion of wall climbing soft robots with a high speed.[153] Here, two dielectric EA pads were tethered via an electroactive actuator which when working in synchronicity can guide the robot to climb walls made of a variety of materials at 90° elevation. Here, the movement of the robot can be controlled by expanding the electroactive polymer with one pad firmly attached and the other loosely attached using the programmable power supply, as shown in Figure 11d. The robot could achieve a speed of 0.75 body length per second as it largely

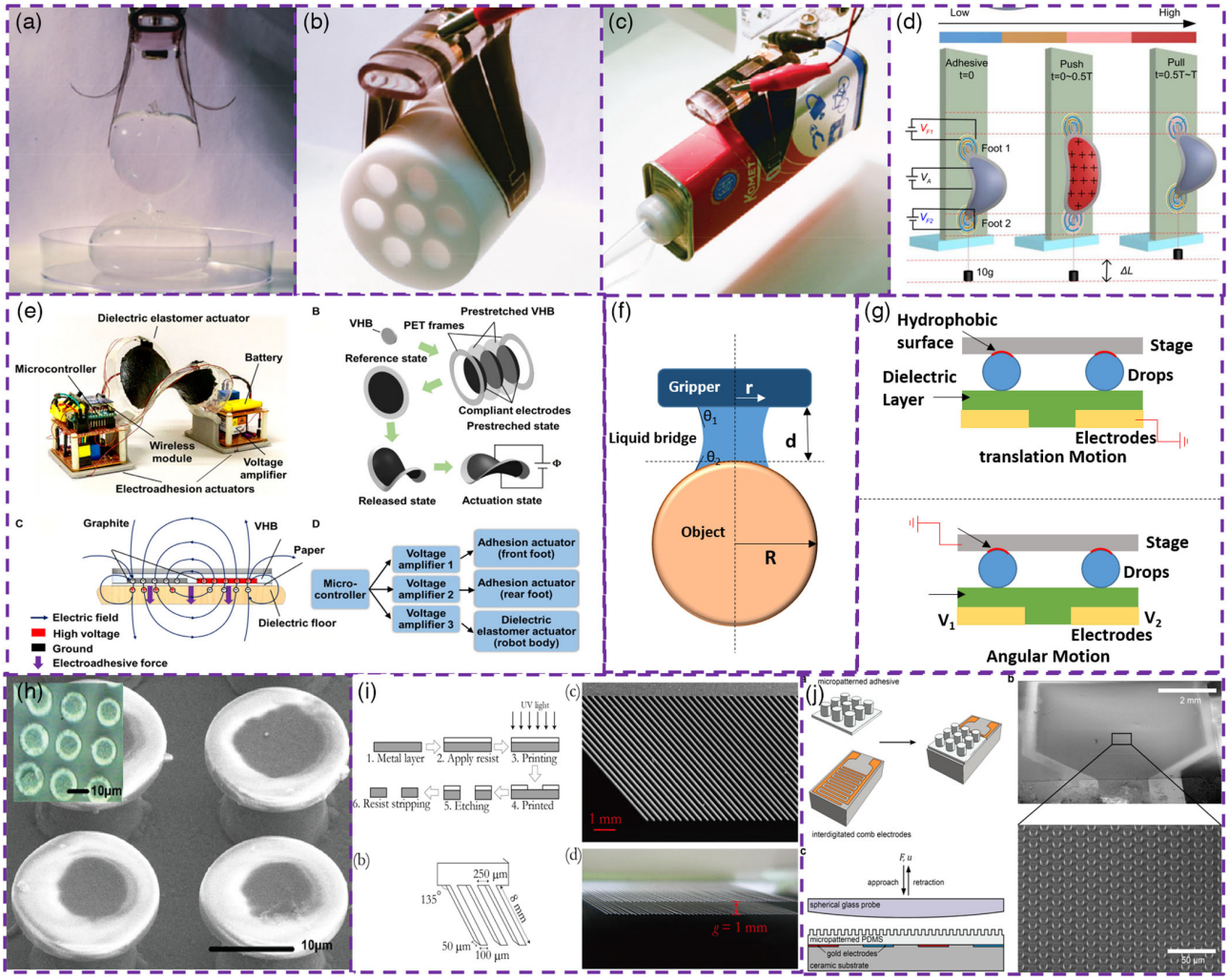

Figure 11. Hybrid EA effects. a) Hybrid EA device lifting a very fragile, highly deformable water-filled thin membrane balloon with relative ease and without puncture; b) demonstration of lifting a Teflon tube; and (c) metallic can be filled with oil using a motorized controller. Reproduced with permission.[59] Copyright 2015, Wiley; d) wall climbing robots with EA pads to hold and electroactive polymer to moving forward or changing direction. Reproduced with permission.[153] Copyright 2018, AAAS; e) intelligent and independent wall climbing robot with internal batteries and amplifiers. Reproduced with permission.[154] Copyright 2018, Elsevier; f,g) devices involving liquid in hybrid EA, (f) illustration of a typical capillary microgripper where a liquid drop can be used to lift objects[91]; (g) (top) schematic for the translation motion; the voltage was supplied to the two electrodes which are separated by a dielectric separator that behaves as a capacitor and for the angular motion; different values of voltage were supplied which resulted in the one drop shifting downward and the other remains unperturbed resulting in the angular motion[165]; f,g) Redrawn from ref [91] and [165]. h–j) gecko-type hybrid EA devices; (h) SEM micrographs of patterned microstructures which has a bulged overhanging outer rim; the simple van der Walls adhesion can be increased with the incorporation of EA technology. Reproduced with permission.[169] Copyright 2012, ACS; (i) schematic of fabrication, device dimensions, and real device SEM images assembly of compliant electrostatic gripper prototype. Reproduced with permission.[173] Copyright 2016, IOP Publishing Ltd; (j) schematic of micropillar gecko adhesive structure made through replica molding and dropped on the IDT electrodes, SEM image, and schematic of the adhesion test setup where a spherical glass was attached and detached at altered applied voltages. Reproduced with permission.[175] Copyright 2020, ACS [https://pubs.acs.org/doi/10.1021/acsami.0c05077, further permissions related to the material excerpted should be directed to the ACS].

depends on the tethering electroactive polymer length and its actuation properties. In fact, by combining multiple parallel units the robot can be made to shift its direction. The force of adhesion was sufficient to carry a small camera which can be very useful in rescue and surveillance missions. Even the robot performance was impressive however, it lacks the simplicity in power requirements as multiple and external units were needed. A similar design was earlier investigated by Jiawei and co-workers where the low-weight batteries and complementary electronics were embedded in the robot EA pads for the locomotion and adhesion.[154,155] As the robot contains all the peripheral electronics mounted, hence, the overall weight was more than usual. Moreover, this allowed them to discuss the effects of coupling and decoupling time due to voltage amplifiers present. A high voltage amplifier that is bulky (large weight) has an RC time constant of orders of a few milliseconds which was suitable for the applications, whereas the low voltage amplifiers that are quite lightweight had the RC time constant close to 1 s. The judicious

use of peripheral electronics is resembled to realize the inchworm-type robot and is shown in Figure 11e. Recently, Geonwoo et al. designed a flexible EA device coupled with multilayered dielectric elastomeric actuators (DEAs) to hold flat as well as round objects more securely and tightly.[77,156] As explained earlier, electroactive polymer expands on applying electrical energy which can be easily converted to large bending motion by multiplying units and securing at its edges during deformation. This will also reinforce the actuator and can lift as many as 100 times their weight. A dynamic pick-and-drop system was realized capable of lifting heavier objects like dumbbells and delicate objects like electric bulbs, glass vials, and bottles of complex shapes and sizes.

6.2. Interesting High Voltage EA Applications Techniques Involving Liquids

Electrorheological fluid is the class of special nanocomposites that contains nano- to microsized particles in the liquid whose rheological properties (flow and deformation) can be controlled by the external electric field. Rienmüller used granular particles for lifting operations.[157] Monkman found that upon using granules the gap persists which reduces the adhesion force and hence he examined the use of electrorheological fluids in EA applications.[20] Shear force due to the fluidic layer has a nonuniform impact where materials like knitted cotton do not show any impact whereas Rayon shows an increase in 100% shear force strength.

EW is a technique for altering the contact angle of small droplets roughly less than 2 mm by the action of high voltages.[158] This technique was developed by Lippmann from the principle of electrocapillarity where the meniscus of liquid (surface energy) has a strong relationship with the surface potential values. Here, the change in surface energy of the liquid with applied potential is proportional to the surface charge density.[159] The alternating voltage allows the small droplets to deform and swiftly move which is commonly referred to as the tap dance of droplets.[159] Moreover, the use of AC voltage and pairs of interdigitated electrodes allow the swift locomotion of drops for a variety of microfluidic and drug delivery applications. In a way, electrowetting is an analogous phenomenon to EA technology and electroactive actuators with a liquid film involved instead of a solid. The device structure is largely the same where a pair of electrodes are covered with a dielectric film (usually hydrophobic) as in EA technology. Though there are many interesting applications of EW like digital microfluidics, Micro Total Analysis Systems, varifocal lenses, optical switches, display technology, and so on, we will highlight only the closely related fields.

Abhay and Jiang designed a microgripper using the EW technology to pick up and drop smaller objects.[91,160] Here, the gripper could pick up small objects like glass beads using a liquid bridge and gripper surface with relatively small force, as shown in Figure 11f. θ_1 and θ_2 are the angles of liquid bridge between the gripper and the object, respectively. The capillarity force can be calculated by $F_{\text{capillarity}} = \frac{\gamma(\cos\theta_1+\cos\theta_2)A}{d}$.

Liquid surface can be manipulated easily by the electric field applied to IDT electrodes below the Teflon layer which is governed by the Young–Lippmann equation. Here, first, the voltage is applied to make the surface hydrophilic and the glass bead is approached. Once the contact is set, the electric field is varied to successfully attach the object to the gripper. The voltage can be lowered to drop the material at the respective locations. However, in the initial experiment, the driving voltage was high; hence. to lower the voltage below 30 V, a well-known dielectric material barium strontium titanate was coated as an interfacial layer which improved the adhesion forces by an order.[91] Similar designs were further researched by others as well.[161] Instead of lifting substrates using this unconventional technique, some researchers even worked on the manipulation of gripping liquid droplets by electrostatic forces and further dropping at the respective locations.[162] Here, a commercial atomic force microscope (AFM) tip was used as a gripper and voltage supplier between the drop and insulating substrate. The volumetric ratio (ratio of the volume of drop before and after gripping) was largely dependent upon θ_1 and θ_2. A theoretical investigation was performed to understand the underpinning principle.

The manipulation of liquid using EW can be employed as microhydraulics which can indirectly be used to lift objects.[163] Here, capillaries of multiple diameters were designed using microfabrication techniques on the Si/SiO_2 substrate (with commercial Cytop coating to make it hydrophobic). The voltage can manipulate and push the liquid across the channels and can work as microhydraulics at the microscale. However, going into details is beyond the scope of the present review and readers can read these interesting articles here.[164] This technology can also be tailored for microscopic angular and spatial manipulators for MEMS applications.[165] In this device, two separate strategies were used for the translation and angular motions. For the translation motion, the voltage was supplied to the two electrodes which are separated by a dielectric separator that behaves as a capacitor, as shown in Figure 11g. However, for the angular motion, different values of voltage were supplied which resulted in the one drop shifting downward and the other remaining unperturbed resulting in the angular motion. Here, we have briefly discussed these technologies with the prospects of creating curiosity in the minds of readers about the allied areas of research potential EA holds for next-generation researchers.

6.3. Van der Walls EA Hybrid Devices

Inspiration from nature is an important part of human development which led to many important discoveries. Researchers were always intrigued by the way Gecko could walk vertically and even in upside-down positions, and proposed many theories.[166] With the advent of electron microscopy, the presence of microscopic features called "Spatulae" (also known as setae) is proved for enhancing the proximity to the surface to allow the van der Wall forces to act and simultaneously provide the necessary adhesion force.[167] Simple gecko adhesion is prone to low load capacity, sensitivity toward surface contaminations like dust and oil, and so on. Hence, to improve the reliability of the normal gecko device, EA can be coupled to improve reliability and large load-carrying capacity. Researchers in this direction used lithography, nanoimprinting, nanodrawing, plasma etching, and so on to fabricate the synthetic setae for the realization of dry adhesives.[168]

In this section, we will discuss the advances in the field of gecko adhesives utilizing EA-T for the hybrid technology.

Jeffrey and Carlo co-utilized the EA with gecko to improve the shear strength of adhesion.[169] Using a nanolithography technique, mushroom cap fibrillar structures were fabricated using the carbon black and PDMS composite, as shown in Figure 11h. The shear strength of the bond was evaluated and further improvements were made using EA technology. A fivefold increment in the shear strength was detected when 4 kV of EA pads were used against the simple gecko device. The output was measured in atmospheric pressure as well as low pressure, increasing its feasibility on earth as well as in space. The setup was built and shown to work for the docking system and can be readily implemented in space stations.[170] Donald et al. designed EA pads below the gecko device using different electrode designs as discussed earlier.[32] The microwedges were fabricated in the SU-8 molds using silicone rubber where the adhesion force increased by fivefold compared to stand-along gecko or EA.[171] To improve the design aesthetics, Jeffrey and co-workers embed the EA electrodes in the dielectric medium and used them for adhering to conductive materials.[172] Nevertheless, most of the existing experiments worked for the adhesion of flat smooth/rough surfaces and missed out the highly curved surfaces. Radon et al. designed the EA pads by embedding the electrodes inside the setae.[104] The outer layer of setae worked as a dielectric medium for EA whereas the shape worked as a gecko gripper. However, it must be added that this increased the size of setae immensely thus largely reducing its original hierarchical biomimetic concept. The design was later modified with quite smaller setae grippers as displayed in Figure 11i.[173] The lithography technique on a metal substrate along with chemical etching was used to fabricate the micropillar network with the smallest dimension of 50 μm. As the electrodes were not shielded with dielectric, the force was quite small. Moreover, the current fabrication technique promoted larger gaps between the individual micropillars which decreased the performance. To overcome this, they used finer lithography of silicon on an insulator (SOI) which is used in semiconductor microfabrication.[102] Rui et al. investigated the feasibility of such devices in the quadruped wall-climbing robotic gecko application[174] where robot paws contain the gecko-designed surface with EA pads allowing it to move independently. As inspired by the natural habitat, the cross-legged configuration can be used for the forward as well as backward movement, and for turning, parallel front and backend limb configuration was utilized.

Recently, Vaishali et al. fabricated a simple design of silicone micropillars with IDT electrode layer beneath demonstrating a coupled gecko EA device, as displayed in Figure 11j.[175] The authors also examined a simulation model which tested out the effects of various parameters like dielectric thickness, the conductivity of medium and elastomer, dielectric constants, electrode geometry, and so on. The hybrid device produced twice as large adhesion as compared to standalone systems and the simulation parameters largely matched the experimental investigations. These mushroom cup or micropillar morphology was proved to be good for adhesion, but the decoupling time was very large due to the nondirectional nature of setae. Dadkhah et al. fabricated the wedge-shaped microgripper whereby switching the direction of load the gripper can be decoupled very easily (16 ms).[176] Also, instead of the IDT electrode design, they implemented a parallel plate capacitor design. The device was energy efficient and worked well on the life cycle test and can be readily used for robotic applications in surveillance and space applications. A similar wedge design with IDT was lately used by Alizadehyazdi et al. to carry fragile and delicate objects.[177] Carbon nanotubes are inherently morphologically analogous to spatulae in gecko feet and are often employed as the dry adhesive.[178] Recently, Michael et al. fabricated the carbon nanotube covered with ultrathin aluminum oxide which makes an interesting biomimetic natural structure without complicated lithography steps.[89] The device achieved the on/off ratio of 700 with an effective distance of ≈3 μm and a maximum adhesive force of 20 kPa. Different materials adhered and the maximum adhesion was the function of dielectric break down in air which is governed by Paschen's law and the dielectric thickness as discussed in Section 2. These hybrid devices are an interesting area of research that improves the existing capability of EA just by morphology variation. It was shown to be used in the real-time space application aboard NASA's C9B zero-gravity airplane.[116]

7. Future Directions and Commercial Remarks

The historical development of EA technology along with various working models is discussed. The perspectives from the materials and fabrication front and the related applications are overviewed. We presented the wider domains of EA devices that are gradually becoming a part of mainstream applications for a prospective future. Grabit Inc. is a recent incubated startup that aims to modernize the existing robotic gripping industry. The products offered will cater to different industries and promise increased safety, increased productivity (up to 20 times), increased loading efficiency (50%), and increased operations density (100%). The grippers are more reliable and reduce damage losses in food, logistics, footwear, apparel, aerospace, electronics, and agriculture industries.[179]

Despite all these advancements, the following key challenges of EA technology are still pending: 1) reduction in the overall voltage of operations; 2) increase the life cycle of the device to at least a million cycles; 3) improve the exteroceptive and proprioceptive functionality; 4) instant coupling and decoupling; 5) reduce fabrication cost and fabrication challenges in Gecko-based adhesion; 6)use of this technology in the construction, mining, and agriculture industry; and 7) design standardization.

Also, it is important to mention the key highlighted areas of cross-disciplinary researchers where EA can be readily implemented in various technologies, such as 1) Life science: cell manipulations; tissue healing; surgeries; separations; drug delivery; microfluidics, and so on. 2) Materials science: 2D materials; nanoparticle arrestors; paints; adhesion promotors; lithography tools, and so on. 3) Mechatronics: constructions sites; automations; rovers; DIY kits, and so on.

The global COVID-19 pandemic has intensified the demand to automate to alleviate workforce challenges and develop operational and food safety in industrial environments. With the further advancement of EA technology, its wider acceptance in industries and automation have foreseen for developing smart

and soft robotics in the areas of navigation systems, textiles, healthcare, and biometric monitoring. Great research opportunities in EA or hybrid EA-based technologies will act as a catalyst to inspire young researchers to develop EA-integrated smart robotics across disciplines.

Acknowledgements

P.R. is thankful to the Talent introduction postdoc fellowship granted by OCPC China and Zhejiang University. P.R. is also thankful to the Haining Municipal Govt. for the postdoc special grant (grant no. 130000-171207723/010) and NSFC young scientist grant (grant no. 52150410426). M.M. is grateful to SERB India for rendering the fellowship from the India-Purdue OVDF program. C.W. thanks for the support of the RSC International Exchange Scheme (IEC\NSFC\191291). This work was supported by the following programs: National Natural Science Foundation of China (grant no. 21927810), Zhejiang Lab (grant no.2018EB0ZX01).

Conflict of Interest

The authors declare no conflict of interest.

Keywords

electroadhesion, grippers, haptics, hybrid adhesion, intelligent robotics

Received: March 9, 2022
Revised: March 26, 2022
Published online:

[1] a) F. A. Johinsen, K. Rabbek, US Patent 311, 385, **1919**; b) R. Knud, Google Patents, **1951**; c) K. Rahbek, US Patent A 1932, 2025123, **1935**.
[2] A. Johnsen, K. Rahbek, *J. Inst. Electr. Eng.* **1923**, *61*, 713.
[3] G. J. Monkman, *Int. J. Rob. Res.* **1997**, *16*, 1.
[4] G. J. Monkman, The University of Hull **1987**.
[5] J. Guo, T. Bamber, M. Chamberlain, L. Justham, M. Jackson, *J. Phys. D: Appl. Phys.* **2016**, *49*, 415304.
[6] X. Liang, Y. Sun, H. Wang, R. C. Yeow, S. L. Kukreja, N. Thakor, H. Ren, presented at *2016 6th IEEE Int. Conf. on Biomedical Robotics and Biomechatronics (BioRob)*, IEEE, Piscataway, NJ **2016**.
[7] K. Wang, Y. Lu, J. Cheng, L. Ji, *Proc. Inst. Mech. Eng., Part C* **2019**, *233*, 302.
[8] J. Guo, J. Leng, J. Rossiter, *IEEE Trans. Rob.* **2019**, *36*, 313.
[9] a) M. Honarpardaz, M. Tarkian, J. Ölvander, X. Feng, *Rob. Auton. Syst.* **2017**, *87*, 104; b) N. Boubekri, P. Chakraborty, Integrated Manufacturing Systems **2002**; c) P. Koustoumpardis, N. Aspragathos, *Hand* **2004**, *19*, 20; d) G. Fantoni, F. Biganzoli, *J. Manuf. Sci. Prod.* **2004**, *6*, 163; e) J. Hughes, U. Culha, F. Giardina, F. Guenther, A. Rosendo, F. Iida, *Front. Rob. AI* **2016**, *3*, 69.
[10] a) https://www.computerhope.com/history/1953.htm, in Other computer events in 1953, 1953 Computer history; b) http://hpmuseum.net/display_item.php?hw=82, HP Computer Museum, Pen Plotters Selection: 9125A Flatbed Plotter, **1956**.
[11] C. J. Fitch, *IBM J. Res. Dev.* **1957**, *1*, 49.
[12] a) A. J. P. Landon, W. B. Pennebaker, H. C. Wang, United States Patent, **1983**; b) A. J. Landon, W. B. Pennebaker, H. C. Wang, Google Patents, **1983**.
[13] G. Program, **1962**; https://nssdc.gsfc.nasa.gov/planetary/gemini.html.
[14] R. P. Krape, *Applications Study of Electroadhesive Devices*, National Aeronautics and Space Administration, Washington, DC, **1968**.
[15] P. Jakhar, A. Kumar, M. Das, P. Rajagopalan, in *CMOS Analog IC Design for 5G and Beyond*, Springer, Berlin **2021**, p. 15.
[16] M. Y.-K. Watanabe, K. Masami, K. Shiro, I. Kenji, K. Kouichi, K. Mitsuaki, S. Takanori, United States Patent, **1997**.
[17] a) A. R. Zias, B. Block, K. W. Mapes, N. L. Nystrom, R. M. Cadwell, Japan Patent JP2782546B2, **1990**; b) Y. Shioya, Y. Oyama, N. Tsuzuki, M. Maeda, M. Ichikawa, F. Mieno, Shin-ichi Inoue, Y. Uo-ochi, A. Tabuchi, A. Tsukune, T. Watanabe, T. Ohba, Korea Patent KR900003612B1, **1987**; c) Takashi YamazakiToshinori Kobayashi, Japan Patent JPH0828205B2, **1989**.
[18] Q. S. R. M. R. K. S. L. J. T. Gardner, United States Patent, **1997**.
[19] a) V. Abrarov, *Sov. Eng. Res.* **1985**, *5*, 37; b) G. J. Monkman, P. M. Taylor, G. J. Farnworth, *Int. J. Clothing Sci. Technol.* **1989**, *1*, 14; c) X. Chen, M. Sarhadi, *Mechatronics* **1992**, *2*, 363.
[20] G. J. Monkman, *Robotica* **1992**, *10*, 183.
[21] T. Nakamura, A. Yamamoto, *Robomech J.* **2017**, *4*, 1.
[22] A. D. Stuckes, *Proc. IEE-Part B: Radio Electron. Eng.* **1956**, *103*, 125.
[23] R. Atkinson, *Br. J. Appl. Phys.* **1969**, *2*, 325.
[24] G. J. Levermore, interface phenomena associated with the Johnsen-Rahbek effect.**1975**.
[25] R. M. Strong, D. E. Troxel, *IEEE Transactions on Man-Machine Systems* **1970**, *11*, 72.
[26] T. Nakamura, A. Yamamoto, presented at *2013 World Haptics Conf. (WHC)*, Daejeon, Korea (South), **2013**.
[27] T. Watanabe, T. Kitabayashi, C. Nakayama, *Jpn. J. Appl. Phys.* **1993**, *32*, 864.
[28] T. Watanabe, T. Kitabayashi, C. Nakayama, *Jpn. J. Appl. Phys.* **1992**, *31*, 2145.
[29] D. J. Meyer, M. A. Peshkin, J. E. Colgate, presented at *2013 World Haptics Conf. (WHC)*, Daejeon, Korea (South), **2013**.
[30] E. Vezzoli, M. Amberg, F. Giraud, B. Lemaire-Semail, presented at *Int. Conf. on Human Haptic Sensing and Touch Enabled Computer Applications*, Versailles, France, **2014**.
[31] a) R. Chen, Y. Huang, Q. Tang, *J. Adhes. Sci. Technol.* **2017**, *31*, 1229; b) R. Chen, Y. Huang, Q. Tang, L. Bai, *J. Adhes. Sci. Technol.* **2016**, *30*, 2301.
[32] a) D. Ruffatto, J. Shah, M. Spenko, presented at *2013 IEEE Aerospace Conference*, Big Sky, MT, USA, IEEE, Piscataway, NJ **2013**; b) D. Ruffatto III, J. Shah, M. Spenko, presented at *Int. Design Engineering Technical Conferences and Computers and Information in Engineering Conference*, Chicago, Illinois, USA, **2012**.
[33] J. Guo, T. Bamber, T. Hovell, M. Chamberlain, L. Justham, M. Jackson, *IFAC-PapersOnLine* **2016**, *49*, 309.
[34] E. Mallinckrodt, A. Hughes, W. Sleator Jr, *Science* **1953**.
[35] B. N. Persson, *J. Phys.: Condens. Matter* **2021**, *33*, 435001.
[36] a) S. Grimnes, *Acta Physiol. Scand.* **1983**, *118*, 19; b) T. Vodlak, Z. Vidrih, E. Vezzoli, B. Lemaire-Semail, D. Peric, *Biotribology* **2016**, *8*, 12.
[37] a) D. J. Beebe, C. Hymel, K. Kaczmarek, M. Tyler, presented at *Proc. of 17th International Conference of the Engineering in Medicine and Biology Society*, Montreal, QC, Canada, **1995**; b) H. Tang, D. J. Beebe, *IEEE Trans. Rehabil. Eng.* **1998**, *6*, 241.
[38] a) H. Hertz, *Ueber die Berührung fester elastischer Körper*, De Gruyter, **2021**; b) V. L. Popov, *Contact mechanics and friction*, Springer, Berlin **2010**.
[39] K. L. Johnson, K. Kendall, A. Roberts, *Proc. R. Soc. London. A* **1971**, *324*, 301.
[40] B. V. Derjaguin, V. M. Muller, Y. P. Toporov, *J. Colloid Interface Sci.* **1975**, *53*, 314.
[41] M. Ciavarella, A. Papangelo, *Front. Mech. Eng.* **2020**, *6*, 27.

[42] a) D. Maugis, *Contact, adhesion and rupture of elastic solids*, Vol. *130*, Springer Science & Business Media, Berlin **2000**; b) D. Maugis, *J. Colloid Interface Sci.* **1992**, *150*, 243; c) P. Prokopovich, S. Perni, *Colloids Surf. A* **2011**, *383*, 95.
[43] B. Persson, *J. Chem. Phys.* **2018**, *148*, 144701.
[44] B. N. Persson, M. Scaraggi, *J. Chem. Phys.* **2014**, *141*, 124701.
[45] A. Almqvist, C. Campana, N. Prodanov, B. Persson, *J. Mech. Phys. Solids* **2011**, *59*, 2355.
[46] B. Persson, A. Kovalev, S. Gorb, *Tribol. Lett.* **2013**, *50*, 17.
[47] M. Ayyildiz, M. Scaraggi, O. Sirin, C. Basdogan, B. N. Persson, *Proc. Natl. Acad. Sci.* **2018**, *115*, 12668.
[48] C. D. Shultz, M. A. Peshkin, J. E. Colgate, presented at *2018 IEEE Haptics Symp. (HAPTICS)*, IEEE, Piscataway, NJ **2018**.
[49] A. Papangelo, M. Ciavarella, *J. R. Soc. Interface* **2017**, *14*, 20160996.
[50] M. Ciavarella, *Meccanica* **2018**, *53*, 241.
[51] a) V. L. Popov, M. Hess, *arXiv preprint arXiv:1805.08714* **2018**; b) J. van Kuilenburg, M. A. Masen, E. van der Heide, *Proc. Inst. Mech. Eng., Part J: J. Eng. Tribol.* **2015**, *229*, 243; c) S. Dalvi, A. Gujrati, S. R. Khanal, L. Pastewka, A. Dhinojwala, T. D. Jacobs, *Proc. Natl. Acad. Sci.* **2019**, *116*, 25484.
[52] C. Basdogan, M. R. A. Sormoli, O. Sirin, *IEEE Trans. Haptics* **2020**, *13*, 511.
[53] a) P. G. Slade, *Electrical Contacts: Principles and Applications*, CRC Press, Boca Raton **2017**; b) D. Tabor, in *Plenary and Invited Lectures*, Elsevier, Amsterdam **1977**, p. 3; c) K. Autumn, M. Sitti, Y. A. Liang, A. M. Peattie, W. R. Hansen, S. Sponberg, T. W. Kenny, R. Fearing, J. N. Israelachvili, R. J. Full, *Proc. Natl. Acad. Sci.* **2002**, *99*, 12252; d) C. Ribeiro, V. Sencadas, D. M. Correia, S. Lanceros-Mendez, *Colloids Surf. B Biointerfaces* **2015**, *136*, 46; e) R. Gohar, H. Rahnejat, *Fundamentals of tribology*, World Scientific, Singapore **2018**; f) F. P. Bowden, F. P. Bowden, D. Tabor, *The Friction and Lubrication of Solids*, Vol. *1*, Oxford University Press, Oxford **2001**.
[54] a) V. L. Popov, in *Multiscale Biomechanics and Tribology of Inorganic and Organic Systems*, Springer, Cham, **2021**, p. 473; b) L. A. Thimons, A. Gujrati, A. Sanner, L. Pastewka, T. D. Jacobs, *Exp. Mech.* **2021**, *61*, 1109; c) A. Tiwari, J. Wang, B. Persson, *Phys. Rev. E* **2020**, *102*, 042803.
[55] X. Li, Y. Ma, C. Choi, X. Ma, S. Chatterjee, S. Lan, M. C. Hipwell, *Adv. Mater.* **2021**, *33*, 2008337.
[56] a) C. Hendriks, S. Franklin, *Tribol. Lett.* **2010**, *37*, 361; b) S. Tomlinson, R. Lewis, X. Liu, C. Texier, M. Carré, *Tribol. Lett.* **2011**, *41*, 283.
[57] M. Li, X. Wang, P. Rajagopalan, L. Zhang, S. Zhan, S. Huang, W. Li, X. Zeng, Q. Ye, Y. Liu, *ACS Appl. Bio Mater.* **2020**, *3*, 8901.
[58] O. Sirin, M. Ayyildiz, B. Persson, C. Basdogan, *Soft Matter* **2019**, *15*, 1758.
[59] J. Shintake, S. Rosset, B. Schubert, D. Floreano, H. Shea, *Adv. Mater.* **2016**, *28*, 231.
[60] K. Choi, Y. Chan Kim, H. Sun, S.-H. Kim, J. W. Yoo, I.-K. Park, P.-C. Lee, H. J. Choi, H. R. Choi, T. Kim, *ACS Omega* **2019**, *4*, 7994.
[61] D. Ruffatto, J. Shah, M. Spenko, *J. Electrostat.* **2014**, *72*, 147.
[62] K. Asano, F. Hatakeyama, K. Yatsuzuka, *IEEE Trans. Ind. Appl.* **2002**, *38*, 840.
[63] W. Saravia, B. Udrea, presented at *2016 IEEE Aerospace Conf.*, IEEE, Piscataway, NJ **2016**.
[64] M. Dadkhah, D. Ruffatto, Z. Zhao, M. Spenko, *J. Electrostat.* **2018**, *91*, 48.
[65] M. Bigharaz, T. Schenkel, P. A. Bingham, *J. Electrostat.* **2021**, *109*, 103540.
[66] G. Monkman, *Ind. Rob.: Int. J.* **2003**, *30*, 326.
[67] Y. Wei, H. Zhou, H. Deng, W. Ji, K. Tian, Z. Ma, K. Zhang, Q. Fu, *Nano-Micro Lett.* **2022**, *14*, 1.
[68] J. Germann, B. Schubert, D. Floreano, presented at *2014 IEEE/RSJ Int. Conf. on Intelligent Robots and Systems*, IEEE, Piscataway, NJ **2014**.
[69] J. Guo, K. Elgeneidy, C. Xiang, N. Lohse, L. Justham, J. Rossiter, *Smart Mater. Struct.* **2018**, *27*, 055006.
[70] R. Chen, R. Song, Z. Zhang, L. Bai, F. Liu, P. Jiang, D. Sindersberger, G. J. Monkman, J. Guo, *Soft Rob.* **2019**, *6*, 701.
[71] C. Cao, X. Gao, J. Guo, A. Conn, *Appl. Sci.* **2019**, *9*, 2796.
[72] X. Gao, C. Cao, J. Guo, A. Conn, *Adv. Mater. Technol.* **2019**, *4*, 1800378.
[73] K. Choi, S.-H. Kim, U. Hwang, J. Kim, I.-K. Park, K.-S. Jang, H. J. Choi, H. R. Choi, T. Kim, J. Suhr, *ACS Appl. Electron. Mater.* **2020**, *2*, 1596.
[74] J. Guo, T. Bamber, J. Petzing, L. Justham, M. Jackson, *Appl. Phys. Lett.* **2017**, *110*, 051602.
[75] J. Guo, M. Tailor, T. Bamber, M. Chamberlain, L. Justham, M. Jackson, *J. Phys. D: Appl. Phys.* **2016**, *49*, 035303.
[76] E. W. Schaler, D. Ruffatto, P. Glick, V. White, A. Parness, presented at *2017 IEEE/RSJ Int. Conf. on Intelligent Robots and Systems (IROS)*, IEEE, Piscataway, NJ **2017**.
[77] G. Hwang, J. Park, D. S. D. Cortes, K. Hyeon, K.-U. Kyung, *IEEE Trans. Ind. Electron.* **2021**, *69*, 642.
[78] P. Rajagopalan, V. Singh, I. A. Palani, *Mater. Res. Bull.* **2016**, *84*, 340.
[79] H. Louati, R. Ouiddir, N. Zouzou, A. Tilmatine, presented at *2020 IEEE Industry Applications Society Annual Meeting*, IEEE, Piscataway, NJ **2020**.
[80] N. Berdozzi, Y. Chen, L. Luzi, M. Fontana, I. Fassi, L. M. Tosatti, R. Vertechy, *IEEE Rob. Autom. Lett.* **2020**, *5*, 2770.
[81] J. Guo, C. Xiang, J. Rossiter, *Mater. Des.* **2018**, *156*, 586.
[82] K. M. Digumarti, C. Cao, J. Guo, A. T. Conn, J. Rossiter, presented at *2018 IEEE Int. Conf. on Soft Robotics (RoboSoft)*, IEEE, Piscataway, NJ **2018**.
[83] K. Zhang, S. Follmer, presented at *2018 IEEE Haptics Symp. (HAPTICS)*, IEEE, Piscataway, NJ **2018**.
[84] N. Berdozzi, Y. Chen, L. Luzi, G. Bocchieri, M. Fontana, I. Fassi, L. M. Tosatti, R. Vertechy, presented at *Electroactive Polymer Actuators and Devices (EAPAD) XXII*, Bellingham, WA, **2020**.
[85] R. Chen, Z. Zhang, R. Song, C. Fang, D. Sindersberger, G. J. Monkman, J. Guo, *Smart Mater. Struct.* **2020**, *29*, 055009.
[86] V. Cacucciolo, J. Shintake, H. Shea, presented at *2019 2nd IEEE Int. Conf. on Soft Robotics (RoboSoft)*, IEEE, Piscataway, NJ **2019**.
[87] M. Caselli, N. Berdozzi, L. Agostini, M. Fontana, I. Fassi, L. M. Tosatti, R. Vertechy, presented at *Electroactive Polymer Actuators and Devices (EAPAD) XXIII*, **2021**.
[88] D. Sindersberger, N. Prem, G. J. Monkman, K. Zimmermann, presented at *ACTUATOR; Int. Conf. and Exhibition on New Actuator Systems and Applications 2021*, Online, **2021**.
[89] M. S. Boutilier, C. Cao, N. Nayakanti, S. Kim, S. M. Taheri-Mousavi, A. J. Hart, *ACS Appl. Mater. Interfaces* **2020**, *13*, 1192.
[90] H. Lim, G. Hwang, K.-U. Kyung, B.-J. Kim, *Smart Mater. Struct.* **2021**, *30*, 035007.
[91] A. Vasudev, J. Zhe, presented at *TRANSDUCERS 2009-2009 Int. Solid-State Sensors, Actuators and Microsystems Conf.,* Denver, CO, USA, **2009**.
[92] A. S. Chen, S. Bergbreiter, *Smart Mater. Struct.* **2017**, *26*, 025028.
[93] G. Xie, W. Wang, X. Zhao, H. Wang, presented at *2019 IEEE 9th Annual Inter. Conf. on CYBER Technology in Automation, Control, and Intelligent Systems (CYBER)*, Suzhou, China, IEEE, Piscataway, NJ **2019**.
[94] a) H. J. Kim, B. Chen, Z. Suo, R. C. Hayward, *Science* **2020**, *367*, 773; b) H. J. Kim, L. Paquin, C. W. Barney, S. So, B. Chen, Z. Suo, A. J. Crosby, R. C. Hayward, *Adv. Mater.* **2020**, *32*, 2000600; c)

J. Zhang, Z. Chen, Y. Zhang, S. Dong, Y. Chen, S. Zhang, *Adv. Mater.* **2021**, 2100962.
[95] J. Fessl, F. Mach, J. Navrátil, *Open Phys.* **2018**, *16*, 430.
[96] C. M. Das, L. Kang, Q. Ouyang, K. T. Yong, *InfoMat* **2020**, *2*, 698.
[97] S. Park, J. Shintake, Y. Piskarev, Y. Wei, I. Joshipura, E. Frey, T. Neumann, D. Floreano, M. D. Dickey, *Adv. Mater. Technol.* **2021**, *6*, 2100263.
[98] G. J. Monkman, S. Hesse, R. Steinmann, H. Schunk, *Robot Grippers*, John Wiley & Sons, Hoboken NJ **2007**.
[99] K. Yatsuzuka, F. Hatakeyama, K. Asano, S. Aonuma, *IEEE Trans. Ind. Appl.* **2000**, *36*, 510.
[100] J. Choi, H. Park, M. K. Son, C.-O. Jeong, W.-B. Kim, *J. Korean Inst. Surf. Eng.* **2016**, *49*, 567.
[101] K. Yatsuzuka, J.-I. Toukairin, K. Asano, S. Aonuma, presented at *Conf. Record of the 2001 IEEE Industry Applications Conf.. 36th IAS Annual Meeting (Cat. No. 01CH37248)*, IEEE, Piscataway, NJ **2001**.
[102] S. Choi, K. Wakabayashi, K. Takahashi, S. Saito, *J. Micromech. Microeng.* **2018**, *28*, 125011.
[103] a) S. Saito, F. Soda, R. Dhelika, K. Takahashi, W. Takarada, T. Kikutani, *Smart Mater. Struct.* **2012**, *22*, 015019; b) J. Berengueres, M. Urago, S. Saito, K. Tadakuma, H. Meguro, presented at *2006 IEEE International Conference on Robotics and Biomimetics*, IEEE, Piscataway, NJ **2006**.
[104] R. Dhelika, K. Sawai, K. Takahashi, W. Takarada, T. Kikutani, S. Saito, *Smart Mater. Struct.* **2013**, *22*, 095010.
[105] S. Yuchun, C. Jia, L. Yijia, H. Yuemin, J. Linhong, *J. Semicond.* **2015**, *36*, 084004.
[106] a) C. Brecher, M. Emonts, B. Ozolin, R. Schares, presented at *19th Int. Conf. on Composite Materials*, IEEE, Piscataway, NJ **2013**; b) G. J. Monkman, *Int. J. Rob. Res.* **1995**, *14*, 144; c) G. J. Monkman, *Robotica* **1996**, *14*, 119.
[107] a) M. F. Grimberg, Google Patents, **2020** US10660402B; b) M. F. Grimberg, EP Patent, **2021** EP3616548.
[108] A. Yamamoto, T. Nakashima, T. Higuchi, presented at *2007 Int. Symp. on Micro-NanoMechatronics and Human Science*, Nagoya, Japan, **2007**.
[109] H. Prahlad, R. Pelrine, S. Stanford, J. Marlow, R. Kornbluh, presented at *2008 IEEE Int. Conf. on Robotics and Automation*, IEEE, Piscataway, NJ **2008**.
[110] R. Chen, R. Liu, H. Shen, presented at *2013 IEEE Workshop on Advanced Robotics and its Social Impacts*, IEEE, Piscataway, NJ **2013**.
[111] J. Mao, L. Qin, Y. Wang, J. Liu, L. Xue, presented at *2014 IEEE Int. Conf. on Mechatronics and Automation*, IEEE, Piscataway, NJ **2014**.
[112] K. H. Koh, M. Sreekumar, S. Ponnambalam, *Mechatronics* **2016**, *35*, 122.
[113] R. Liu, R. Chen, H. Shen, R. Zhang, *Int. J. Adv. Rob. Syst.* **2013**, *10*, 36.
[114] Q. Wu, V. Pradeep, X. Liu, presented at *2018 IEEE Int. Conf. on Soft Robotics (RoboSoft)*, IEEE, Piscataway, NJ **2018**.
[115] a) M. Ritter, D. Barnhart, presented at *2017 IEEE Aerospace Conf.*, Wailea, Maui, Hawaii, IEEE, Piscataway, NJ **2017**; b) B. C. Leung, N. R. Goeser, L. A. Miller, S. Gonzalez, presented at *2015 IEEE Aerospace Conf.*, IEEE, Piscataway, NJ **2015**; c) T. Bryan, T. Macleod, L. Gagliano, S. Williams, B. McCoy, presented at *Advanced Maui Optical and Space Surveillance Technologies Conf.*, **2015**.
[116] P. Aaron, S. Russell, F. Christine, W. Nicholas, K. Simon, R. Donald, D. Mohammad, K. Jaakko, C. Kalind, S. Matthew, in *66rd Int. Astronautical Congress*, Vol. *IAC-15-A2.3.1*, The International Astronautical Federation, Jerusalem, Israel **2015**.
[117] M. Graule, P. Chirarattananon, S. Fuller, N. Jafferis, K. Ma, M. Spenko, R. Kornbluh, R. Wood, *Science* **2016**, *352*, 978.
[118] L. K. Borden, A. Gargava, S. R. Raghavan, *Nat. Commun.* **2021**, *12*, 1.
[119] A. B. Vankov, P. Huie, M. S. Blumenkranz, D. V. Palanker, presented at *Ophthalmic Technologies XIV*, San Jose, CA, United States, **2004**.
[120] a) R. Hinchet, H. Shea, *Adv. Mater. Technol.* **2020**, *5*, 1900895; b) M. Gareis, J. Maas, presented at *ACTUATOR; Int. Conf. and Exhibition on New Actuator Systems and Applications 2021*, **2021**; c) J. Li, Y. Xiong, B. Yang, K. Ma, X. Tao, Available at SSRN 3931629; d) E. Leroy, R. Hinchet, H. Shea, *Adv. Mater.* **2020**, *32*, 2002564; e) X. Ji, X. Liu, V. Cacucciolo, Y. Civet, A. El Haitami, S. Cantin, Y. Perriard, H. Shea, *Adv. Funct. Mater.* **2021**, *31*, 2006639.
[121] V. Alizadehyazdi, M. Bonthron, M. Spenko, *J. Electrostat.* **2020**, *108*, 103499.
[122] V. Alizadehyazdi, M. Modabberifar, S. J. Mahmoudzadeh Akherat, M. Spenko, *J. R. Soc. Interface* **2018**, *15*, 20170714.
[123] V. Alizadehyazdi, E. McQueney, K. Tanaka, M. Spenko, presented at *2018 IEEE/RSJ Int. Conf. on Intelligent Robots and Systems (IROS)*, IEEE, Piscataway, NJ **2018**.
[124] Y. Okuno, H. Shigemune, Y. Kuwajima, S. Maeda, *Adv. Mater. Technol.* **2019**, *4*, 1800304.
[125] J. Lee, W. Jeon, Y. Cha, H. Yang, presented at *2017 IEEE/RSJ Int. Conf. on Intelligent Robots and Systems (IROS)*, IEEE, Piscataway, NJ **2017**.
[126] a) C. Shultz, M. Peshkin, J. E. Colgate, *IEEE Trans. Haptics* **2018**, *11*, 279; b) J. Mullenbach, M. Peshkin, J. E. Colgate, *IEEE Trans. Haptics* **2016**, *10*, 358.
[127] C. D. Shultz, M. A. Peshkin, J. E. Colgate, presented at *2015 IEEE World Haptics Conf. (WHC)*, IEEE, Piscataway, NJ **2015**.
[128] a) J. V. Vidal, V. Slabov, A. L. Kholkin, M. P. S. Dos Santos, *Nano-Micro Lett.* **2021**, *13*, 1; b) V. Slabov, S. Kopyl, M. P. S. Dos Santos, A. L. Kholkin, *Nano-Micro Lett.* **2020**, *12*, 1.
[129] S. Huang, L. Shi, T. Zou, H. Kuang, P. Rajagopalan, H. Xu, S. Zhan, J. Chen, W. Xuan, H. Jin, *Adv. Mater.* **2020**, *10*, 2002470.
[130] a) H. Kuang, Y. Li, S. Huang, L. Shi, Z. Zhou, C. Gao, X. Zeng, R. Pandey, X. Wang, S. Dong, *Nano Energy* **2021**, *80*, 105561; b) G. Khandelwal, A. Chandrasekhar, R. Pandey, N. P. M. J. Raj, S.-J. Kim, *Sens. Actuators B: Chem.* **2019**, *282*, 590; c) V. Vivekananthan, A. Chandrasekhar, N. R. Alluri, Y. Purusothaman, G. Khandelwal, R. Pandey, S.-J. Kim, *Nano Energy* **2019**, *64*, 103926; d) P. Rajagopalan, S. Huang, L. Shi, H. Kuang, H. Jin, S. Dong, W. Shi, X. Wang, J. Luo, *Nano Energy* **2021**, *80*, 105560; e) P. Rajagopalan, V. Singh, I. A. Palani, S.-J. Kim, *Extreme Mech. Lett.* **2019**, *26*, 18; f) B. Dong, Q. Shi, Y. Yang, F. Wen, Z. Zhang, C. Lee, *Nano Energy* **2021**, *79*, 105414; g) M. Zhu, Z. Yi, B. Yang, C. Lee, *Nano Today* **2021**, *36*, 101016; h) Z. Sun, M. Zhu, C. Lee, *Nanoenergy Adv.* **2021**, *1*, 81; i) Z. Sun, M. Zhu, Z. Zhang, Z. Chen, Q. Shi, X. Shan, R. C. H. Yeow, C. Lee, *Adv. Sci.* **2021**, *8*, 2100230; j) M. Zhu, Z. Sun, T. Chen, C. Lee, *Nat. Commun.* **2021**, *12*, 1.
[131] M. Muthu, R. Pandey, X. Wang, A. Chandrasekhar, I. A. Palani, V. Singh, *Nano Energy* **2020**, *78*, 105205.
[132] A. Ahmed, I. Hassan, M. F. El-Kady, A. Radhi, C. K. Jeong, P. R. Selvaganapathy, J. Zu, S. Ren, Q. Wang, R. B. Kaner, *Adv. Sci.* **2019**, *6*, 1802230.
[133] L. Xu, H. Wu, G. Yao, L. Chen, X. Yang, B. Chen, X. Huang, W. Zhong, X. Chen, Z. Yin, *ACS Nano* **2018**, *12*, 10262.
[134] J. Nie, Z. Ren, J. Shao, C. Deng, L. Xu, X. Chen, M. Li, Z. L. Wang, *ACS Nano* **2018**, *12*, 1491.
[135] a) L. Zheng, Y. Wu, X. Chen, A. Yu, L. Xu, Y. Liu, H. Li, Z. L. Wang, *Adv. Funct. Mater.* **2017**, *27*, 1606408; b) J. Nie, T. Jiang, J. Shao, Z. Ren, Y. Bai, M. Iwamoto, X. Chen, Z. L. Wang, *Appl. Phys. Lett.* **2018**, *112*, 183701.
[136] J. Nie, Z. Ren, Y. Bai, J. Shao, T. Jiang, L. Xu, X. Chen, Z. L. Wang, *Adv. Mater. Technol.* **2019**, *4*, 1800300.

[137] J. Yu, X. Wei, Y. Guo, Z. Zhang, P. Rui, Y. Zhao, W. Zhang, S. Shi, P. Wang, *Lab Chip* **2021**, *21*, 284.
[138] T. Bu, H. Yang, W. Liu, Y. Pang, C. Zhang, Z. L. Wang, *Soft Rob.* **2019**, *6*, 664.
[139] C. Fang, Y. Cao, D. Jiang, J. Tian, C. Zhang, *Microsyst. Nanoeng.* **2020**, *6*, 1.
[140] X. Chen, X. Pu, T. Jiang, A. Yu, L. Xu, Z. L. Wang, *Adv. Funct. Mater.* **2017**, *27*, 1603788.
[141] X. Chen, Y. Wu, A. Yu, L. Xu, L. Zheng, Y. Liu, H. Li, Z. L. Wang, *Nano Energy* **2017**, *38*, 91.
[142] L. Zheng, S. Dong, J. Nie, S. Li, Z. Ren, X. Ma, X. Chen, H. Li, Z. L. Wang, *ACS Appl. Mater. Interfaces* **2019**, *11*, 42504.
[143] D. Yang, X. Kong, Y. Ni, Z. Ren, S. Li, J. Nie, X. Chen, L. Zhang, *Nano Energy* **2019**, *66*, 104139.
[144] J. Guo, T. Bamber, Y. Zhao, M. Chamberlain, L. Justham, M. Jackson, *IEEE Rob. Autom. Lett.* **2016**, *2*, 538.
[145] C. Xiang, J. Guo, J. Rossiter, *Smart Mater. Struct.* **2019**, *28*, 055034.
[146] W. Peisong, H. Ting, Z. He, W. Yang, L. Qing, W. Zhen, F. Xiao, W. Fang, W. Peng, S. Chongxin, F. Zhiyong, L. Lei, Z. Peng, H. Weida, *InfoMat* **2022**, *4*, e12275.
[147] J. Biggs, K. Danielmeier, J. Hitzbleck, J. Krause, T. Kridl, S. Nowak, E. Orselli, X. Quan, D. Schapeler, W. Sutherland, *Angew. Chem., Int. Ed.* **2013**, *52*, 9409.
[148] G. Kofod, W. Wirges, M. Paajanen, S. Bauer, *Appl. Phys. Lett.* **2007**, *90*, 081916.
[149] Y. Bar-Cohen, V. Cardoso, C. Ribeiro, S. Lanceros-Méndez, *Advanced Piezoelectric Materials* Second Edition Chapter 8-Electroactive Polymers as Actuators, **2017**, p. 319.
[150] I.-S. Park, K. Jung, D. Kim, S.-M. Kim, K. J. Kim, *MRS Bull.* **2008**, *33*, 190.
[151] a) L. Hines, K. Petersen, G. Z. Lum, M. Sitti, *Adv. Mater.* **2017**, *29*, 1603483; b) J. Shintake, V. Cacucciolo, D. Floreano, H. Shea, *Adv. Mater.* **2018**, *30*, 1707035; c) Y. Bar-Cohen, *Electroactive polymer (EAP) actuators as artificial muscles: reality, potential, and challenges*, Vol. *136*, SPIE press, Bellingham **2004**; d) Y. Bar-Cohen, I. A. Anderson, *Mech. Soft Mater.* **2019**, *1*, 1; e) S. I. Rich, R. J. Wood, C. Majidi, *Nat. Electron.* **2018**, *1*, 102; f) I. A. Anderson, T. A. Gisby, T. G. McKay, B. M. O'Brien, E. P. Calius, *J. Appl. Phys.* **2012**, *112*, 041101.
[152] B. Sun, X. Zhang, presented at *2019 IEEE 15th Int. Conf. on Automation Science and Engineering (CASE)*, IEEE, Piscataway, NJ **2019**.
[153] G. Gu, J. Zou, R. Zhao, X. Zhao, X. Zhu, *Sci. Rob.* **2018**, *3*.
[154] J. Cao, L. Qin, J. Liu, Q. Ren, C. C. Foo, H. Wang, H. P. Lee, J. Zhu, *Extreme Mech. Lett.* **2018**, *21*, 9.
[155] J. Cao, L. Qin, H. P. Lee, J. Zhu, presented at *Electroactive Polymer Actuators and Devices (EAPAD) 2017*, Portland, Oregon, United States, **2017**.
[156] G. Hwang, J. Park, D. S. D. Cortes, K.-U. Kyung, presented at *2020 3rd IEEE Int. Conf. on Soft Robotics (RoboSoft)*, IEEE, Piscataway, NJ **2020**.
[157] T. Rienmüller, H. Weissmantel, presented at *Int. Symp. on Industrial Robots*, Lausanne, Switzerland, **1988**.
[158] F. Mugele, J.-C. Baret, *J. Phys.: Conden. Matter* **2005**, *17*, R705.
[159] Y.-P. Zhao, Y. Wang, *Rev. Adhes. Adhes.* **2013**, *1*, 114.
[160] A. Vasudev, J. Zhe, presented at *2008 17th Biennial University/Government/Industry Micro/Nano Symp.*, Louisville, KY, USA, **2008**.
[161] G. Fantoni, H. N. Hansen, M. Santochi, *CIRP Ann.* **2013**, *62*, 17.
[162] B. Bhushan, X. Ling, *J. Phys.: Condens. Matter* **2008**, *20*, 485009.
[163] J. Kedzierski, K. Meng, T. Thorsen, R. Cabrera, S. Berry, *J. Microelectromech. Syst.* **2016**, *25*, 394.
[164] a) J. Kedzierski, E. Holihan, *Science Rob.* **2018**, *3*; b) J. Kedzierski, E. Holihan, R. Cabrera, I. Weaver, *Microsyst. Nanoeng.* **2017**, *3*, 1; c) J. Kedzierski, H. Chea, *Microsyst. Nanoeng.* **2021**, *7*, 1.
[165] D. J. Preston, A. Anders, B. Barabadi, E. Tio, Y. Zhu, D. A. Dai, E. N. Wang, presented at *2017 IEEE 30th Int. Conf. on Micro Electro Mechanical Systems (MEMS)*, IEEE, Piscataway, NJ **2017**.
[166] T. F. E. Wikipedia, *Wikipedia, the free encyclopedia*, **2001**.
[167] K. Autumn, Y. A. Liang, S. T. Hsieh, W. Zesch, W. P. Chan, T. W. Kenny, R. Fearing, R. J. Full, *Nature* **2000**, *405*, 681.
[168] a) A. P. Russell, A. Y. Stark, T. E. Higham, *Integr. Comp. Biol.* **2019**, *59*, 101; b) K. Autumn, P. H. Niewiarowski, J. B. Puthoff, *Ann. Rev. Ecol. Evol. Syst.* **2014**, *45*, 445; c) Y. Li, J. Krahn, C. Menon, *J. Bionic Eng.* **2016**, *13*, 181.
[169] J. Krahn, C. Menon, *Langmuir* **2012**, *28*, 5438.
[170] F. Branz, L. Savioli, A. Francesconi, F. Sansone, J. Krahn, C. Menon, presented at *6th European Conf. on Space Debris, ESA/ESOC*, Darmstadt, Germany, **2013**.
[171] D. Ruffatto, A. Parness, M. Spenko, *J R Soc. Interface* **2014**, *11*, 20131089.
[172] J. Krahn, A. Pattantyus-Abraham, C. Menon, *Proc. Inst. Mech. Eng., Part L: J. Mater.: Des. Appl.* **2014**, *228*, 109.
[173] R. Dhelika, P. Hemthavy, K. Takahashi, S. Saito, *Smart Mater. Struct.* **2016**, *25*, 055037.
[174] R. Chen, R. Liu, J. Chen, J. Zhang, presented at *2013 IEEE Int. Conf. on Robotics and Biomimetics (ROBIO)*, IEEE, Piscataway, NJ **2013**.
[175] V. Chopra, M. Chudak, R. Hensel, A. A. Darhuber, E. Arzt, *ACS Appl. Mater. Interfaces* **2020**, *12*, 27708.
[176] M. Dadkhah, Z. Zhao, N. Wettels, M. Spenko, presented at *2016 IEEE/RSJ Int. Conf. on Intelligent Robots and Systems (IROS)*, Daejeon, Korea (South), **2016**.
[177] V. Alizadehyazdi, M. Bonthron, M. Spenko, *IEEE Rob. Autom. Lett.* **2020**, *5*, 4679.
[178] a) X. Li, D. Tao, H. Lu, P. Bai, Z. Liu, L. Ma, Y. Meng, Y. Tian, *Surf. Topogr.: Metrol. Prop.* **2019**, *7*, 023001; b) L. Qu, L. Dai, *Adv. Mater.* **2007**, *19*, 3844; c) S. Hu, Z. Xia, L. Dai, *Nanoscale* **2013**, *5*, 475.
[179] a) https://grabitinc.com/products/; b) H. Prahlad, R. J. Casler, S. Kim, M. Leettola, J. Smith, K. Tan, P. Wang, J. M. Farren, P. C. Regan, P. C. Chen, Google Patents, **2021**; c) H. Prahlad, R. J. Casler, S. Kim, M. Leettola, J. Smith, K. Tan, P. Wang, J. M. Farren, P. C. Regan, P. C. Chen, Google Patents, **2018**.
[180] J. D. West, J. Mici, J. F. Jaquith, H. Lipson, *J. Phys. D: Appl. Phys.* **2020**, *53*, 435302.
[181] J. Germann, M. Dommer, R. Pericet-Camara, D. Floreano, *Adv. Rob.* **2012**, *26*, 785.
[182] K. H. Koh, M. Sreekumar, S. Ponnambalam, *Materials* **2014**, *7*, 4963.

Pandey Rajagopalan is a senior postdoctoral fellow at Zhejiang University China and works in nanoelectronics for sensing, energy harvesting, and robotics applications. He is a recipient of several awards including NSFC young scientist award, Talent interdiction Fellow, IKRI Fellow, and so on. He completed his Ph.D. in discipline of MEMS, Indian Institute of Technology Indore, India. He is passionate about energy harvesting and micro/nanodevice fabrication for sustainable technology.

Jikui Luo is a national distinguished professor at Zhejiang University, China. He is the inventor of 13 international patents and has published over 300 peer-reviewed papers, and given over 220 talks at international conferences. He has chaired and cochaired several international conferences and was the co-editor-in-chief of the International Journal of Nanomanufacture and is the associate editor for Sensors and Electronics (MDPI), the Chinese Journal Of Sensors and Actuators, and is a guest editor for seven special issues on MEMS, sensors, and energy harvesting. In past, he held positions at prestigious universities like the University of Cambridge, the University of Bolton, and Cardiff University.

Xiaozhi Wang is an associate professor in the College of Information Science and Electronic Engineering, Zhejiang University China. He worked as a postdoctoral researcher at Microsystem Technology Laboratory, Department of Electrical Engineering and Computer Science, MIT, and received his Ph.D. in electrical engineering at the University of Cambridge, UK. He is interested in the miniaturization of analytical instruments, design, and fabrication of micro–nanodevices and systems, bio-, and flexible electronic devices and systems.

Chaoying Wan received her Ph.D. degree in materials science from Shanghai Jiao Tong University. She was awarded a Marie Curie Individual Fellowship and worked at Trinity College Dublin, Ireland. She joined the University of Warwick, UK in 2012, where she is currently a reader in multifunctional nanocomposites. She specializes in polymer synthesis, characterization, and reactive processing of multiphase/multicomponent nanocomposites, self-healing dielectric elastomers, biodegradable polymers, and sustainable rubbers for energy applications.